Acousto Optic Modulated Stroboscopic Interferometer for Comprehensive Characterization of Microstructure

Murali Manohar Pai S

A Thesis

In

The Department

Of

Mechanical and Industrial Engineering

Presented In Partial Fulfillment of the Requirements

for the Degree of Master of Applied Science (Mechanical Engineering) at

Concordia University

Montreal, Quebec, Canada

April, 2008

© Murali Manohar Pai S, 2008

Library and Archives Canada

Published Heritage Branch

395 Wellington Street
Ottawa ON K1A 0N4
Canada

Bibliothèque et Archives Canada

Direction du Patrimoine de l'édition

395, rue Wellington
Ottawa ON K1A 0N4
Canada

Your file Votre référence
ISBN: 978-0-494-40918-3
Our file Notre référence
ISBN: 978-0-494-40918-3

NOTICE:
The author has granted a non-exclusive license allowing Library and Archives Canada to reproduce, publish, archive, preserve, conserve, communicate to the public by telecommunication or on the Internet, loan, distribute and sell theses worldwide, for commercial or non-commercial purposes, in microform, paper, electronic and/or any other formats.

AVIS:
L'auteur a accordé une licence non exclusive permettant à la Bibliothèque et Archives Canada de reproduire, publier, archiver, sauvegarder, conserver, transmettre au public par télécommunication ou par l'Internet, prêter, distribuer et vendre des thèses partout dans le monde, à des fins commerciales ou autres, sur support microforme, papier, électronique et/ou autres formats.

The author retains copyright ownership and moral rights in this thesis. Neither the thesis nor substantial extracts from it may be printed or otherwise reproduced without the author's permission.

L'auteur conserve la propriété du droit d'auteur et des droits moraux qui protège cette thèse. Ni la thèse ni des extraits substantiels de celle-ci ne doivent être imprimés ou autrement reproduits sans son autorisation.

In compliance with the Canadian Privacy Act some supporting forms may have been removed from this thesis.

Conformément à la loi canadienne sur la protection de la vie privée, quelques formulaires secondaires ont été enlevés de cette thèse.

While these forms may be included in the document page count, their removal does not represent any loss of content from the thesis.

Bien que ces formulaires aient inclus dans la pagination, il n'y aura aucun contenu manquant.

Dedicated to My Beloved amma, appa, jayakka, rajikka and babrai

"All truths are easy to understand once they are discovered; the point is to discover them."

--Galileo Galilei

Italian Philosopher and Mathematician (1564-1642)

ABSTRACT

Acousto Optic Modulated Stroboscopic Interferometer for Comprehensive Characterization of Microstructure

Murali Manohar Pai Sreenivasan

Mechanical and electro-mechanical advancements to the nano-scale require comprehensive and systematic testing at the micro-scale in order to understand the underlying influences that define the micro/nano-device both from fabrication and operational points of view. In this regard, surface metrology measurements, as well as static and dynamic characteristics will become very important and need to be experimentally determined to describe the system fully. These integrated tests are difficult to be implemented at dimensions where interaction with the device can seriously impact the results obtained. Hence, a characterization method to obtain valid experimental information without interfering with the functionality of the device needs to be developed. In this work, a simple yet viable Acousto Optic Modulated Stroboscopic Interferometer (AOMSI) was developed using a frequency stabilized Continuous Wave (CW) laser together with an Acousto Optic Modulator for comprehensive mechanical characterization to obtain surface, static and dynamic properties of micro-scale structures. An optimized methodology for measurement was established and sensitivity analysis was conducted. Being a whole-field technique, unlike single point or scanning interferometers, AOMSI can provide details of surface properties as well as displacements due to static/dynamic loads and modal profiles. Experiments for surface

profiling were carried out on a micro-mirror, along with 2D and 3D profile measurements. The ability of AOMSI to perform dynamic measurements was tested on Micro-Cantilevers and on AFM (Atomic Force Microscopy) cantilevers. The resolution of AOMSI was identified as 10nms. The results for static deflections, 1st and 2nd natural frequencies and mode shapes were found to be in good agreement with results from the developed theoretical model and manufacturers specifications. The approach is a novel approach to investigate the surface, static and dynamic behavior of microstructures using a single interferometer.

ACKNOWLEDGEMENT

I would like to express my sincere thanks and gratitude to my supervisors Dr. Narayanswamy Sivakumar and Dr. Muthukumaran Packirisamy for their unwavering encouragement. I am grateful to Dr. Sivakumar for sharing this knowledge in optical metrology and for his support and advice to setup the Interferometer. I am also grateful to him to show the beacon of hope with his immense knowledge during the experimental phase. I am also very grateful to Dr. Packirisamy for sharing his knowledge on designing of MEMS device and his feedback on the experimental setup. Their genuine enthusiasm for this research topic created an atmosphere that was truly instrumental in the success of this work. I would also like to thank both the supervisors who encouraged me to attend and showcase the research in various conferences. It was a pleasure and privilege to carry out research under them.

I Thank Dr. Petre Tzenov, Dan Juras, Charlene Wald, Arlene and other members of the Department of Mechanical Engineering for their support and advice during the program.

A special thanks to Dr.Gino Rinaldi for his technical expertise in modeling of microstructures. I would like to acknowledge my colleagues Ashwin, Arvind, Raghvendra, Kiran in the Optical Microsystem Laboratory, Ramak ,Chakameh in Laser Micromachining and Metrology Laboratory for all the support and discussions. Also I like to acknowledge Vamshi Raghu and Rohit Singh for their emotional support for the success of the thesis.

My parents and other members in my family deserve a warm and special acknowledgement for their unbounded love and encouragement.

Table of Contents

List of Figures ix

List of Tables xii

List of Symbols xiii

Chapter 1 Introduction

1.1 Introduction 1

1.2 History of Micro Electro Mechanical Systems (MEMS) 1

1.3 Trends in Micro Electro Mechanical Systems (MEMS) 2

1.4 Factors Affecting the Growth of MEMS 4

1.5 Introduction to Characterization Tools in MEMS 6

1.6 Importance of Mechanical Characterization in MEMS 6

1.7 Classification of Characterization Tools in MEMS 7

1.8 Non-Optical Methods 7

1.9 Optical Based Method 10

1.10 Focus Sensing Techniques 10

1.11 Interferometric Techniques 12

1.12 Interferometric Techniques for Surface Profile and Static Behavior 12

1.13 Interferometric Techniques for Dynamic Characterization 13

1.14 Laser Doppler Vibrometer (LDV) 14

1.15 Whole Field Technique 16

1.16 Stroboscopic Interferometer 17

1.17 Acousto Optic Modulator (AOM) in Stroboscopy 18

1.18 Working of Acousto Optic Modulator (AOM) 19

1.19 Digital Laser Microinterferometer 21

1.20 Processing Techniques on a Fringe Pattern 22

1.21 Fringe Tracking 23

1.22 Temporal Phase Measurement/Temporal Heterodyning 24

1.23 Fourier Transform 25

1.24 Objective and Scope of the Thesis 26

Chapter 2 Design and Modeling of MEMS device

2.1 Introduction 27

2.2 Rayleigh-Ritz Method 27

2.3 Energy Formulation 28

2.4 Theoretical Formulation 29

2.5 Modeling the Static Behaviour 29

2.6 Modeling the Dynamic Behaviour 33

2.7 Summary 37

Chapter 3 Experimental Setup of Acousto Optic Modulated Stroboscopic Interferometer

3.1 Introduction 38

3.2 Basic Layout of the Interferometer 39

3.3 Systematic Design and Alignment of the Optical System 42

3.4 Fringe Analysis using Fourier Transformation 44

3.5 Sensitivity Analysis 47

3.5 Optimization of Measurement Method 51

3.4 Summary 53

Chapter 4 Surface Metrology and Static Characterization

4.1 Introduction 54

4.1 Surface Metrology 54

4.2 Surface Metrology on a Connecting Pads 58

4.3 Importance of Static Characterization 59

4.4 AOMSI for Low Frequency Static Characterization 62

4.5 Measurement of Static Deflections 64

4.6 Summary 69

Chapter 5 Dynamic Characterization

5.1 Introduction 70

5.2 Dynamic Characterization 71

5.3 Identification of Natural Frequency 73

5.4 Characterization of mode shapes 75

5.5 Summary 80

Chapter 6 Conclusion

6.1 Conclusion 81

6.2 Future Work 82

References 84

Appendix

List of Journal and Conference 96

List of Figures

Figure 1.1 SEM image of gyroscope 3

Figure 1.2 (a) SEM image of internal stress induced MEMS plate 5

Figure 1.3 Schematic layout of Scanning Electron Microscope [24] 8

Figure 1.4 Classifications of optical techniques 10

Figure 1.5 Full-field white light confocal microscope [25] 11

Figure 1.6 Schematic layout of Mirau interferometric technique [27] 13

Figure 1.7 Schematic layout of LDV [34] 15

Figure 1.8 Schematic of stroboscopic interferometer system [29] 17

Figure 1.9 Working regime of an Acousto Optic Modulator 20

Figure 1.10 Modulation graph of AOM [64] 20

Figure 1.11 Schematic layout of digital laser microinterferometer [41] 22

Figure 1.12 Fringe tracking method 23

Figure 1.13 Interferogram of different known phase shifts 24

Figure 2.1 Schematic of an electrostatically actuated microcantilever 28

Figure 2.2 Equivalent microcantilever with artificial springs 29

Figure 2.3 Static deflection 32

Figure 2.4 Analytical Representations of the 1st and 2nd Mode Shapes 36

Figure 3.1 Schematic overview of the principal components in AOMSI 41

Figure 3.2 Digital image of the layout of the AOMSI assembly 42

Figure 3.3 (a) Interferogram (b) Spectrum image of the interferogram 45

Figure 3.4 (a) Band-pass filter mask (b) Inverse transform image of the interferogram 46

Figure 3.5 2D profile of the discontinuous image 46

Figure 3.6 2D profile of the continuous profile 47

Figure 3.7 Planar wave interference 48

Figure 3.8 Angle between reference mirror and object mirror 49

Figure 3.9 Sensitivity Data of the System 51

Figure 3.10 Ra Value of the micro mirror for various number fringes 52

Figure 4.1 Torsional scanning μ-mirror fabricated using MicraGeM SOI technology 55

Figure 4.2 Fringe pattern from surface of the torsional micro-mirror 56

Figure 4.3 Wrapped image after the inverse analysis of the Fourier transform method 56

Figure 4.4 2D and 3D information of the micro-mirror with the tilt information 57

Figure 4.5 2D Profile of the surface of the torsional micro-mirror 57

Figure 4.6 Surface characteristics obtained for the SOI torsional micro-mirror 58

Figure 4.7 (a) Interferogram (b) Surface information of the surface 59

Figure 4.8 Low frequency excitation using a piezo-stack 61

Figure 4.9 Methodology for static characterization of vibrating microstructures 63

Figure 4.10 Microscopic image of the micragem SOI technology cantilever 65

Figure 4.11 An SEM image of an SOI MicraGem technology cantilever array 65

Figure 4.12 Fringe patterns obtained for the DUT at various voltages 66

Figure 4.13 Static deflection comparisons 67

Figure 5.1 SEM image of the AFM cantilever 70

Figure 5.2 Methodology to conduct dynamic characterization 72

Figure 5.3 Digital image of the interferometer during dynamic characterization 75

Figure 5.4 The observed fringe pattern obtained seen on AFM cantilevers 77

Figure 5.5 Surface profile of a resonating AFM cantilever in the 1st mode 78

Figure 5.6 Surface profile of a resonating AFM cantilever in the 2nd mode 79

List of Tables

Table 1.1 Comparison of non-optical characterization methods for MEMS 9

Table 1.2 Comparison of different fringe processing techniques 26

Table 2.1 Specification of the SOI MicraGem cantilever 31

Table 2.2 Theoretical tip deflection for static characterization 32

Table 2.3 Specification of AFM cantilever 35

Table 2.4 Theoretical resonance frequency 35

Table 3.1 Tabulation of number of fringes to out of plane displacement 50

Table 4.1 Tip deflection of the DUT for static characterization 68

Table 5.1 Comparison of natural frequency 74

List of Symbols

A	Area
cm	Centimeter
C	Capacitance
C_d	Damping factor
C_{dc}	Critical damping factor
d	Distance
d_0	Dielectric gap
E	Young's modulus of elasticity
f	Frequency
$\hat{F}$	Geometry conditioning function
GPa	GigaPascal
h	Material thickness
H	Height
Hz	Hertz
I	Moment of inertia
kg	Kilogram
kHz	Kilohertz
k_E	Electrostatic spring stiffness
K_E	Electrostatic spring stiffness
K_R	Rotational spring stiffness
K_T	Translation spring stiffness
L	Length

m	Meter
mm	Millimeter
M	Mass
MHz	MegaHertz
nm	Nanometer
N	Newton
t	Time
T	Temperature
U_B	Strain energy
U_E	Electrostatic potential energy
U_{ED}	Electrostatic dynamic potential energy
U_{MAX}	Maximum potential energy
V	Voltage
V_1^*	Voltage (non-dimensionalized)
V_2^*	Voltage (non-dimensionalized)
w	Material width
$w(x)$	Positional width
$W(x)$	Flexural deflection
$W_S(x)$	Static Deflection
W_0	Unconditional Width
x	Non-dimensionalized coordinate
y	Non- dimensional co-ordinate

ε	Coefficient of thermal dependence for Young's modulus
ε_0	Permittivity of free space
ε_r	Relative permittivity of a given medium
$\phi_0(x)$	Parent polynomial in x
$\phi_i(x)$	ith orthogonal polynomial in x
$\phi_j(x)$	jth orthogonal polynomial in x
$\phi_i'(x)$	First derivative of ith orthogonal polynomial in x
$\phi_j'(x)$	First derivative of jth orthogonal polynomial in x
$\phi_i''(x)$	Second derivative of ith orthogonal polynomial in x
$\phi_j''(x)$	Second derivative of jth orthogonal polynomial in x
ϕ	Phase Value
λ_K	Eigenvalue
λ	Wavelength
μm	Micrometer
π	Pi
ρ	Material density
ω	Frequency

Chapter 1

Introduction

1.1 Introduction

Micro Electro Mechanical Systems (MEMS) are miniaturized devices with mechanical components with features in the range of few μm and integrated with electronic circuitry for signal processing and analysis. The versatility of MEMS has been the driving force for next generation sensors, actuators and transducers in recent times. The field of MEMS as it is known in North America is also known as Micro System Technology (MST) in Europe and as Micromachines in Japan [1]. Over the years since its implementation, MEMS have found its application in various fields from automobile to biological sensing and some are yet to be uncovered.

1.2 History of Micro Electro Mechanical Systems (MEMS)

The integrated circuit (IC) technology is the starting point in the history of Microsystems. Microfabrication for these IC technologies was developed with a level of fierceness unmatched to other fields. These microfabrication technologies were rapidly matured over the decades from early 1960's. The field of microelectromechanical systems (MEMS) was evolved as an off-shoot of these technologies. Several IC processing technologies were used to make micromechanical devices that included cantilevers, membranes and nozzles. Crucial elements like microsensor, including piezoresistivity of silicon were discovered, studied and optimized [3,7,4]. The bulk micromachining and

surface micromachining technologies [9,10,12] produced sensors at low cost that produced large impact on various products such as ink-jet printers manufactured by Hewlett-Packard which work on silicon micromachined ink-jet printer nozzle in [14,13]. In 1989, first silicon surface micromachined micro-motor using the principle of electrostatic force was demonstrated at University of California at Berkeley [15]. These developments played a significant role in bringing MEMS to broader scientific community and industries. In 1990s, MEMS grew rapidly with government and private funding for research in various applications from optical attenuation in telecommunication to biological studies using MEMS based miniature tools. Early research in companies like Analog devices and Texas Instrument started to bear results for their invention in inertia sensors and projection display. At present the trend is still on to compose lab-on-a-chip to miniaturize analysis system in medical application. Nano Electro-Mechanical System (NEMS) is on a threshold to make unprecedented sensitivity and selectivity of detection [16,17,18,76,78].

1.3 Trends in Micro Electro Mechanical Systems (MEMS)

Outcome of the above mentioned applications made scientific society to create a separate platform dedicated to research on MEMS. The developed Microfabrication and micromachining process was customized to produce MEMS devices [79,81,82,75]. Processes developed offered significant advantages over macroscopic electro-mechanical sensors, principally high sensitivity and low noises. Its Bulk micromachining [80] advantage helped the sensor and other commercial application markets on a spin with low-cost manufacturing with high sensitivity. Advance feature integration with ultra high

sensitivity [19,20] are been offered. Today, one can find variety of micromachined accelerometer sensors with various sensing principles like capacitive sensing [20], piezoresistivity, optical sensing [21] have been demonstrated.

Its multi-disciplinary application from biomedical to aerospace has made researchers customize their approach in development of MEMS device to satisfy their needs. In the next 10 to 20 years the MEMS research is expected to continue its rapid growth curve with advancements in several aspects: (1) An increased functional reach of MEMS in interdisciplinary applications; (2) the maturation of design methodology and fabrication technology; (3) the enhancement of mechanical performances such as sensitivity and robustness; (4) a lowered development cost and cost of ownership [78,77]. Figure 1.1 shows SEM image of a gyroscope designed by the author to sense change in angle.

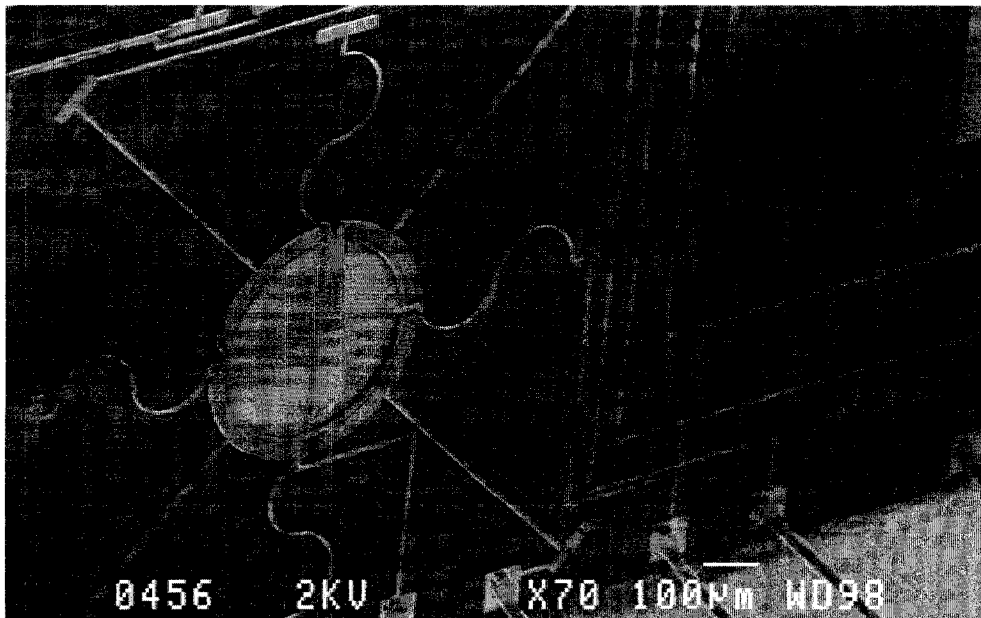

Figure 1.1 SEM image of gyroscope

1.4 Factors Affecting the Growth of MEMS

From the talk given by Richard Feynman about "There is plenty of room at the bottom" scientific community [16] developed a whole new area of getting miniaturized. The factors that affect this growth are in developing new principles and theories that predict the models in micro or nano scale [22]. The models were simulated for various parameters and quantified. Since it is an electromechanical system the device was characterized for electrical and mechanical properties. Scientific community always needs a well proven feedback system to optimize their design either of the fabrication techniques or system. This feedback system is a main factor that helps in the advancement of further development. To create a feedback system, better characterization tools have to be developed for understanding various properties [92,87]. Characterization plays an important role in connecting the link between the theoretical and experimental research [89]. It gives the actual performances of the system. It can predict the failure and other responses which can be used in further development of the design. Figure 1.2 shows the SEM image of internal stress induced in the MEMS design due to fabrication technique and design compensation made to reduce the internal stress.

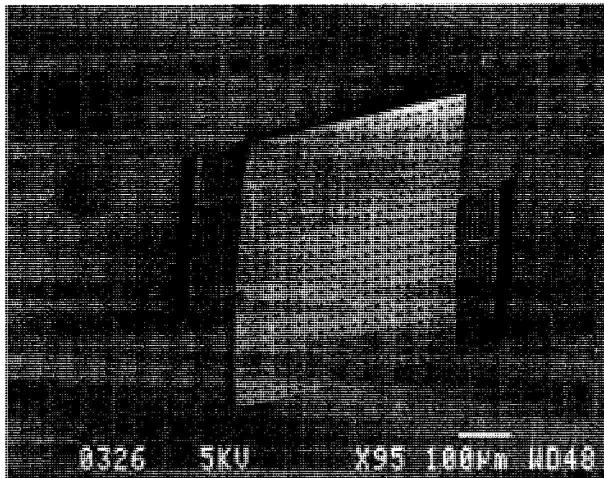

(a)

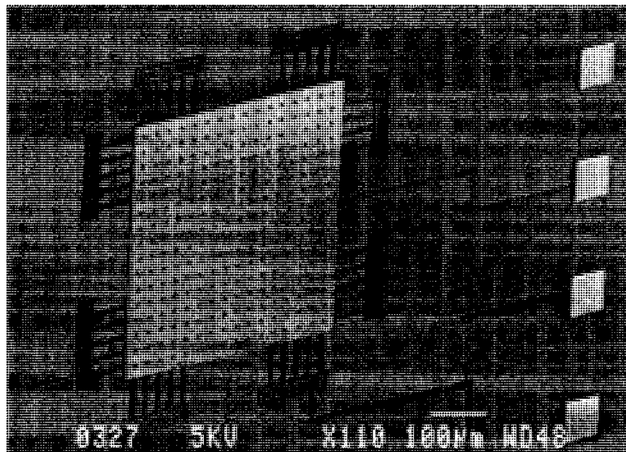

(b)

Figure 1.2 (a) SEM image of internal stress induced MEMS plate (b) Design compensation on the MEMS plate.

1.5 Introduction to Characterization Tools in MEMS

Since the scope of the thesis is within the limits of the characterization of static and dynamic behavior of the MEMS device, attention is drawn to various tools available to characterize mechanical behavior of the MEMS devices in their working environment. The parameters that need to be measured are out-of-plane motion, natural frequency, in-plane motion and modal shape analysis. Other properties that need to be characterized are surface metrology to understand the surface roughness of the material after it is either deposited or fabricated on to a system.

1.6 Importance of Mechanical Characterization in MEMS

Micro Electro Mechanical System (MEMS) involves integration of electronics and mechanical systems. The factors affecting the performances of MEMS devices have equal effect from both systems (mechanical and electronics). Therefore optimization of mechanical system needs tools which can characterize the mechanical behavior to study the change in sensitivity or performances with change in design of its boundary conditions or structure. Device level metrology plays an important role in characterizing the parameters that governs the design of these microstructures. The important parameters are surface roughness of the microstructure that governs the optical attenuation properties [77,78] static behavior of these microstructures under various working environments and sensitivity of these microstructures on loads with its maximum capability to handle these loads. In MEMS devices, loads can be applied using external forces (thermal or pressure) or electro-static force in the system [84]. Another important parameter to characterize is the dynamic behavior in order to understand the

resonance frequency of the microstructure which is usually very high compared to macro systems and mode shapes in resonance frequency.

1.7 Classification of Characterization Tools in MEMS

The tools to characterize these microstructures are non-contact and non-destructive methods. The ability to view and characterize these microstructures can be done either through a microscope or other optical methods. Bosseboeuf et al [23] discuss about the trends of many optical techniques for out-of-plane motions that are the latest trends built using sophisticated electronic devices in order to visualize these microstructures in its static or dynamic motion, tools available to characterize can be classified into non-optical methods [24] and optical methods [23].

1.8 Non-Optical Methods

The most common of the non-optical methods is Scanning Electron Microscope (SEM) [24]. From the discovery of electron to be used for imaging using electron backscattered diffraction images, SEM [24,58] was invented. These microscopes gave a new trend in visualization to view material in sub nanometer resolution, providing minute details of the structure under test. The other non-optical method was using probes to give the surface topography, where microscopes build using tunneling and magnetic principles were employed. The various types of Non-Optical microscope are Scanning Capacitance microscope (SCM)[90], Atomic Force Microscope (AFM) [60], Scanning Probe Microscope (SPM), Scanning Tunneling Microscope (STM)[91], Tunneling

ElectronMicroscope (TEM), in addition to SEM. Figure 1.3 shows the schematic layout of an SEM.

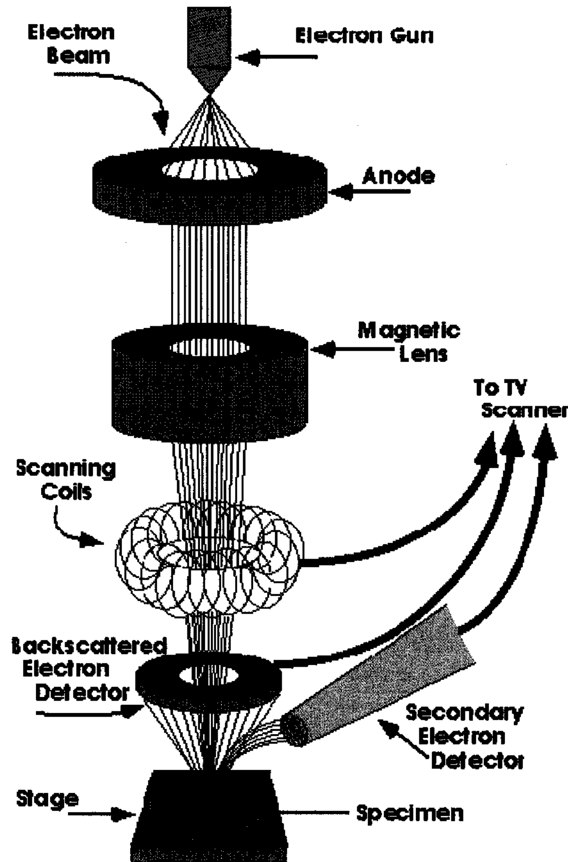

Figure 1.3 Schematic layout of Scanning Electron Microscope [24]

The Table 1.1 below shows the capability of these non-optical microscopes. These microscopes have unique ability to visualize at high resolution but are expensive instruments, need rigorous sample preparation and skilled operations.

	SEM/TEM	SPM/AFM
Operation	Vacuum	Air, Liquid, High Vacuum
Depth of Field	Large	Medium
Later Resolution	1-5nm-SEM 0.1nm-TEM	2-10nm –AFM 0.1nm – STM
Vertical Resolution	N/A	0.1 nm – AFM 0.01nm- STM
Magnification	$10X-10^6X$	$5x10^2X- 10^8X$
Sample	Un-chargeable, vacuum compatible thin film:TEM	Surface height < 10mm
Contrast	Scattering, diffraction	Tunneling

Table 1.1 Comparison of non-optical characterization methods for MEMS

Moreover the non-optical approaches mentioned here are used for surface profile measurement [58,59] but that fail to understand the static and dynamic behavior of microstructure in real time. Optical techniques described by Bossebouef. A et al [23] show a promising trend in developing characterization tools for static and dynamic behavior.

1.9 Optical Based Method

Optical characterization techniques developed for the assessment of microstructure [42] have promising trend to develop low-cost, high resolution, high sensitivity instruments to conduct static and dynamic behavior of microstructure at high speed under normal environments. The inclusion of CCD sensor and software integration with this hardware makes the system more versatile in testing for various parameters. Optical based characterization tools can be classified into two main categories as shown in Figure1.4 focus sensing and interferometric techniques.

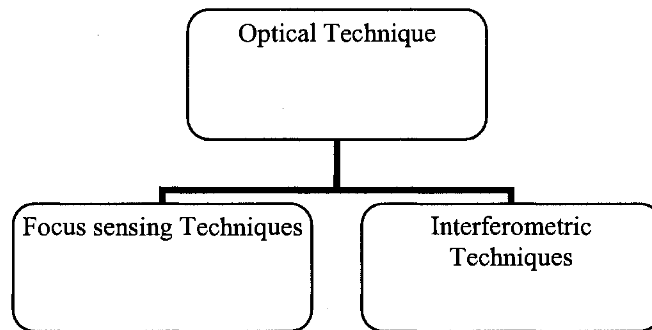

Figure 1.4 Classifications of optical techniques

1.10 Focus Sensing Techniques

Optical microscope is the common focus sensing device. It magnifies the object under test to a given order. Many principles like epifluorescence are used in characterizing microstructures (microchannels) [93]. To be mentioned is confocal microscope which is an important type of focus sensing technique. Its a replacement of diamond tip stylus to an optical stylus to scan the surface profile of a microstructure or can be used for

understanding static behavior of microstructures in full-field [25,26]. It is one of the most important focus sensing technique for surface profiling for structures in micro-regime and other materials (biological and bio-medical) [107]. Gu M et al [25] proposed a scanning system confocal microscope to record various sections of a microstructure using CCD and then to reconstruct them in 3D profiles. Figure 1.5 shows the schematic layout of the confocal microscope. The disc is spiral configuration of various pinholes (Nipkow disc) helps in deleting the out-of-focus information for better imaging, a CCD camera is used to capture the image and white light source for focusing images.

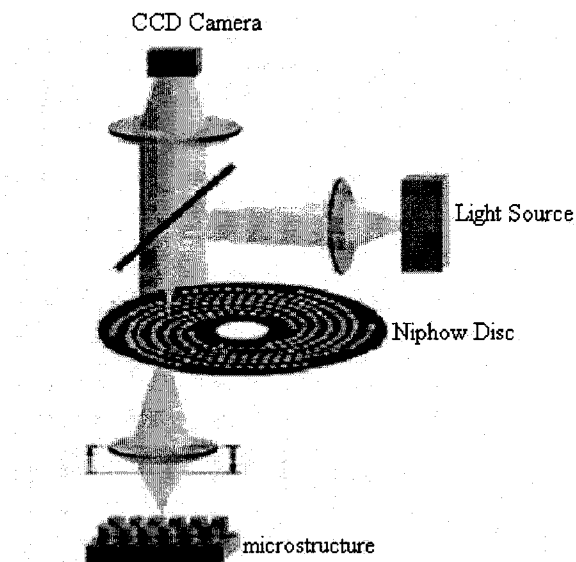

Figure 1.5 Full-field white light confocal microscope [25]

While microscopes are mainly focused for 3D profile information, interferometric techniques developed are most widely used due its capability to conduct characterization for surface information, static and dynamic behavior.

1.11 Interferometric Techniques

Interferometric techniques are an extension of focus sensing technique by using the concept of interference of light [94,95,97]. Analyzing the surface or other parameters like motion and frequency using interferogram is the basis of an interferometric technique. An interferogram is recorded by interference signal between two or more beams of light exciting from the same radiation source. Interference usually refers to the interaction of two or more light waves [95]. An interferometer is an optical setup to create required interferences. Depending on the applications, a suitable interferometer is used to create an interferogram. Christian Rembe et al [30] review the various trends on optical interferometric techniques to study the dynamic behavior of the MEMS. Bossebouf. A et al [23] also review various trends developed to study the surface information and static behavior of MEMS devices. Some of the techniques used in MEMS are reviewed below.

1.12 Interferometric Techniques for Surface Profile and Static Behavior

Assessment of surface profile of microstructure is important in fabrication process optimization for designing of microstructure. Static behavior characterization gives the information of performances of microstructure under static loads. Microscopic interferometry are widely used for the same with most common configuration using monochromatic or white light source such as a Michelson, Mirau or Linnik interferometric methods. C.Quan et al [27] developed an experimental setup with Mirau

objective to understand the nanoscale deformation of MEMS structures. A schematic layout of the experimental setup of the optical system is shown in Figure 1.6. The technique was to develop a microscope with a mirau objective to obtain fringe pattern with the structure for measurement of surface profile and static deflection.

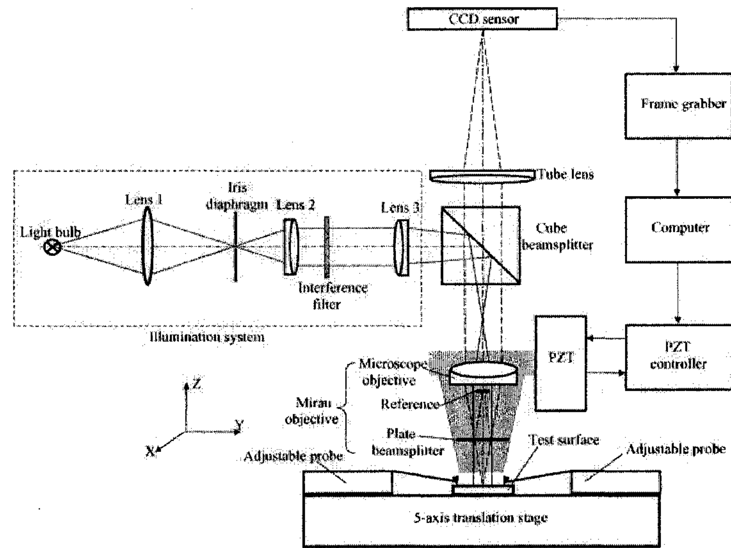

Figure 1.6 Schematic layout of Mirau interferometric technique [27]

The system developed showed the feasibility to understand the 3D deformation and surface contour measurements for microstructures, but unable to perform dynamic characterization.

1.13 Interferometric Techniques for Dynamic Characterization

Dynamic characterization of microstructure leads to measurement of dynamic properties of microstructure while it is vibrating and modal analysis of the microstructure at high frequencies. Advances in optical methodology to develop tools to measure microstructure

made a noteworthy development. Laser Doppler Vibrometer (LDV) which is used for dynamic characterization of macrostructure was implemented into micro level [35,34,36,37]. P.Kehl et al [28] introduced high speed visualization to develop diagnostic tool for microstructure. M.Hart et al [29,31] developed stroboscopic interferometer using LED (Light Emitting Diode) for dynamic characterization. Osten,W et al [32] developed stroboscopic holographic systems to record digital hologram[33] of structures at dynamic state. The details of the dynamic characterization both with their relative pros and cons are discussed below.

1.14 Laser Doppler Vibrometer (LDV)

Laser Doppler Vibrometer works on the principle of Doppler effects to remotely acquire the vibration velocities. Vibration induces a Doppler shift on the incident laser beam. This frequency shift is linearly related to the velocity component in the direction of laser beam. A relationship is established between the laser beam frequency variations with that of the object velocity. To isolate this Doppler shift to understand the dynamics of microstructures interferometry techniques are implemented. A scheme of a Vibrometer incorporating a Mach-Zender interferometer is shown below in Figure 1.7

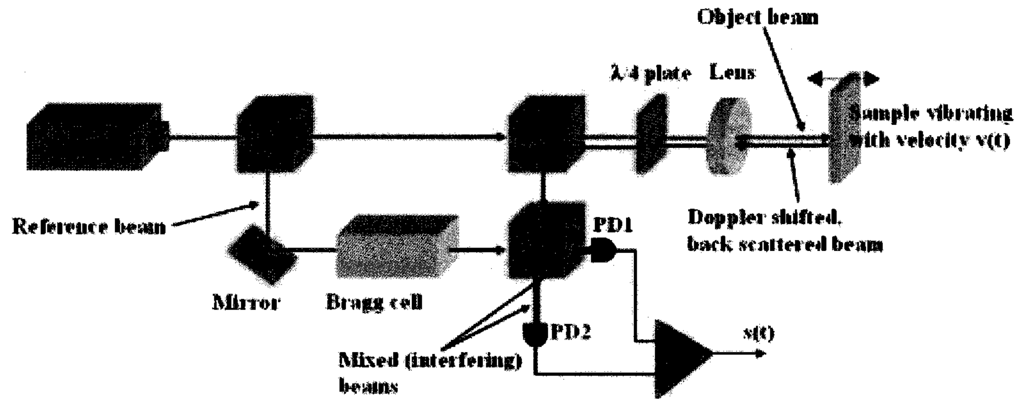

Where BS1, BS2, BS3 are beam splitter, λ/4 is quarter wave plate and PD1, PD2 are photodetector's

Figure 1.7 Schematic layout of LDV [34]

The light from the laser is split into a "reference beam" and an "object (measurement) beam" by beam splitter BS1. The object beam passes through beam splitter BS3 and is focused to a point on the vibrating object by the lens. The backscattered light is diverted by BS3 towards BS2. At BS2, the backscatter from the object mixes together (interferes) with the frequency shifted reference beam. To isolate this frequency heterodyne interferometric technique is implemented [34]. Heterodyne interferometry observes the interferences between two beams with slightly different optical frequencies. This frequency difference is usually achieved by introducing a frequency shift into one of the beams which is created by the Bragg cell [70,100] in the optical setup. Vibrometer usually employ He-Ne lasers. Finally, the optical signal is converted to an electrical signal by photo detectors PD1 and PD2. When the two beams interfere in a photodetector its records a traveling interferences signal at the beat frequency. The LDV is widely used for dynamic characterization of microstructures. Its limits the technique only on a

vibrating body, which makes it not viable for surface profile or static characterization. One of the first commercial dynamic characterization tools was developed based on LDV by Polytec^{TM} Inc. In the latest product it has a capability to detect up to 20MHz signal with scanning system to predict more precisely the dynamic property of a whole device [71,72]. Since LDV is either single point system [37] or scanning system [34,73] it removes the real time assessment [38, 29] and does not have a method to visualize the motion at higher frequency. Being a single point measurement, the position of the laser beam along the device can also misdirect the results (eg: at nodal point in second or higher mode analysis).To visualize these motion and to extract dynamic parameters of the whole device in real-time, whole -field approach would be a better solution [101].

1.15 Whole Field Technique

There is a need for a static and dynamic characterization tool which can visualize the whole system. Opting for non-optical system is expensive and time intense. An optical system with Doppler principle can be reliable but it is either point or scanning method for testing and cannot be used for static behaviors and it is not a whole field technique. The implementation of interferometric technique with a suitable interferometer to measure the phase of whole system is feasible. To make it compatible for dynamic behavior we can use the principle of stroboscopic imaging [39,40]

1.16 Stroboscopic Interferometer

Stroboscopy is an alternative method [62,63] for high speed visualization[98] of cyclic motions. Instead of using an expensive high-speed CCD camera to capture the motion of vibrating body, the light is pulsed at the same frequency at which the object is vibrating. In this method a normal 30 Hz CCD camera is sufficient to capture these motions. C.Rembe et al [40] developed a stroboscopic interferometer at BASC (Berkeley Sensor& Actuator Center) to measure in-plane and out-of-plane displacement in a single experiment. The motion was measured with out-of-plane resolution in the order of 5nm. The setup had capability to strobe laser at 1 MHz. Figure 1.8 is the schematic layout of the stroboscopic interferometer developed at BASC [29].

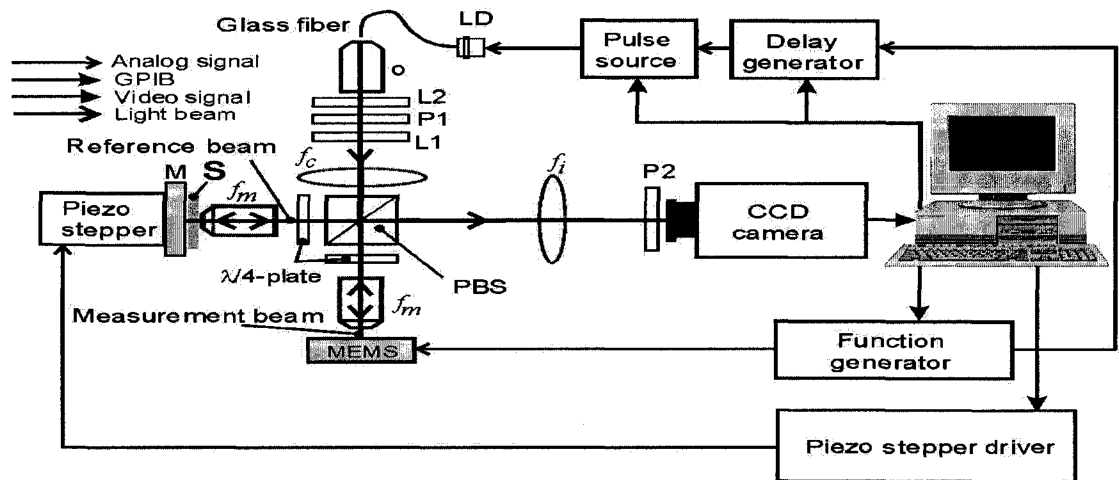

Where L – λ/2 -wave-plate, P– polarizer, PBS – polarization beam splitter, f_c– condenser lens, f_i – imaging lens, and f_m – microscope objective for imaging, LD – laser diode, M – reference mirror

Figure 1.8 Schematic of stroboscopic interferometer system [29]

The interferometer was built on using LED as a source on a Twyman-Green interferometer [102] platform with a CCD camera connected to a frame grabber card. The

pulsing and the driving frequencies of the microstructure were controlled using a computer and the capturing of the motion was done using software. The post processing of the interferogram was done using phase-shifting method. In phase shifting method there is a need to capture images of the same motion at different phases. Even though a better resolution is obtained using this method it complicates the system. Moreover PZT based phase shifting induces mechanical errors which is compensated by algorithms. The strobing is done using a pulse generator on a LED whose reliability fails at higher frequencies. Moreover LEDs are not monochromatic and have restrictions in coherence length and frequency stability. Use of Acousto-Optic Modulator is feasible to get a He-Ne laser source to strobe. He-Ne laser are monochromatic of light at 632.8 nm, unlike LED they are frequency stabilized which is important for high precision metrology [64,99].

1.17 Acousto Optic Modulator (AOM) in Stroboscopy

The laser system that emits continuous wave of monochromatic light are not expensive and comes in lower power ranges is best suited for interferometric process [42]. To strobe continuous wave laser, shutters are required. Common methods of strobing include mechanical/electronic shutters that are good at lower frequencies. The electronic shutters available are in few KHz ranges [108]. At higher frequencies there are LED modules. The dynamic range on MEMS device is between few KHz to few MHz. Alternative methods with ability to strobe at higher frequencies is necessary. AOM is widely used for modulation in telecommunication [68], in heterodyne interferometers (Bragg cell) for frequency variation and acoustic switching on high power pulsed laser [53], non-

mechanical scanning [38]. AOM with low random access time can be used for strobing a laser in high frequency range.

1.18 Working of Acousto Optic Modulator (AOM)

The modulation in an Acousto Optic Modulator is based on the elasto-optic effect, where the change in refractive index of the material is based on the strain. With acoustic waves having sinusoidal properties there is grating effect caused on the crystal which diffracts the light at various orders [65]. A parameter is called the "quality factor, Q", determines the interaction regime. Q is given by

$$Q = \frac{2\pi\lambda\, L}{n\Lambda} \tag{1.1}$$

where λ is the wavelength of the laser beam, n is the refractive index of the crystal, L is the distance the laser beam travels through the acoustic wave and Λ is the acoustic wavelength.

For Q<<1 : This is the Raman-Nath regime. The laser beam is incident roughly normal to the acoustic beam and there are several diffraction orders as shown in Figure 1.9. For Q>>1 : This is the Bragg regime. At one particular incidence angle Θ_B, only one diffraction order is produced the others are annihilated by destructive interference as shown is Figure 1.9. Where Θ_B is defined by

$$\Theta_B = \sin^{-1}\left(\frac{\lambda F}{2v}\right) \tag{1.2}$$

Where F is acoustic frequency and v is the acoustic velocity and λ is the wavelength of the laser [69,65,64].

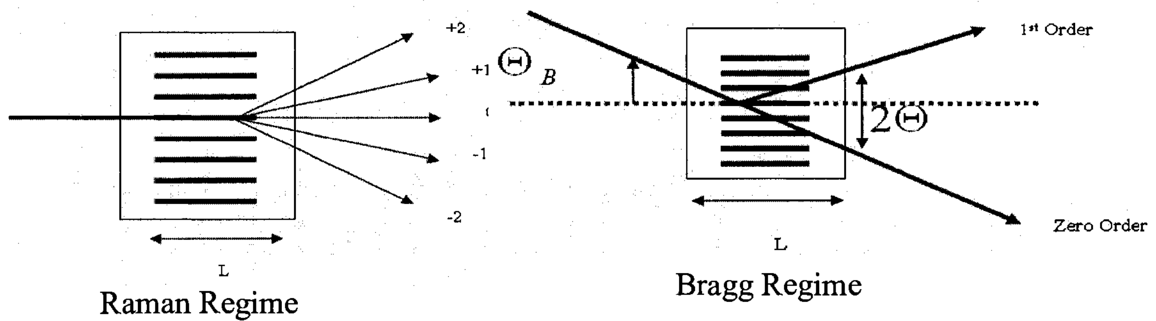

Figure 1.9 Working regime of an Acousto-Optic Modulator

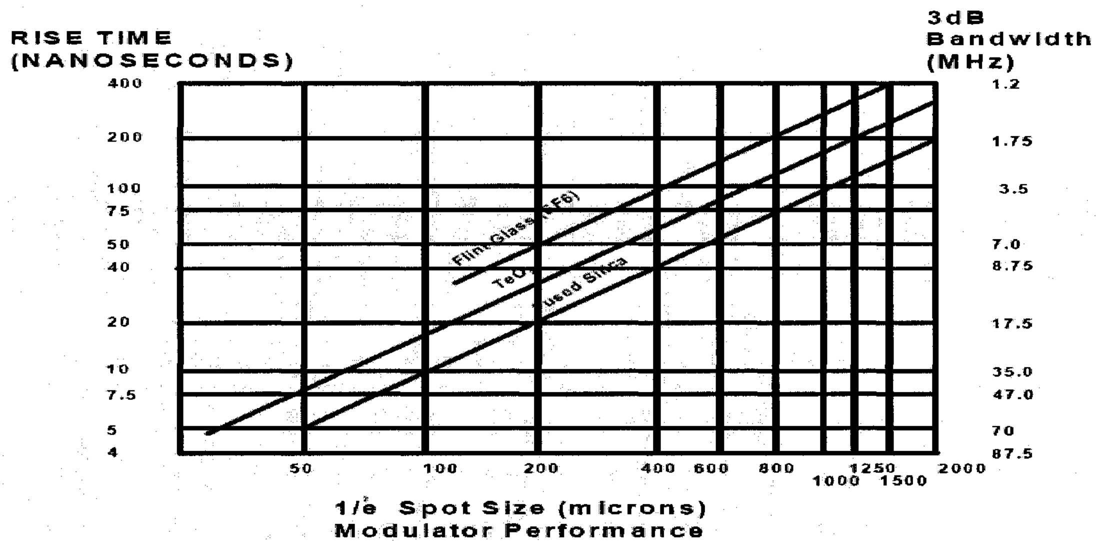

Figure 1.10 Modulation graph of AOM [64]

For the experimental setup in the thesis the AOM is positioned in Bragg angle with respect to laser and the first order beam is used in the classical interferometer. A TeO_2 crystal is used for the modulator with the modulation frequency fixed at 85MHz.In the

experiment 632.8 nm laser is converted from continues wave (CW) to pulsed wave using AOM in combination with a TTL signal generator. The beam size of the laser is 500 μm which is given as the input to the AOM, as per the graph in Figure 1.10 a maximum modulation capacity of 4 MHz for the given beam size is expected. With the decrease of the beam diameter in the input side of AOM a modulation of up to 70 MHz can be achieved [64]. The principle of AOM to strobe the light was implemented in digital laser microinterferometer which is discussed further.

1.19 Digital Laser Microinterferometer

L.Yang et al[41] developed a digital laser microinterferometer using AOM to strobe the laser, together with a Michelson interferometer to implement an electronic speckle pattern interferometry. Speckle interferometry uses the speckle patterns to get the information of the test object. It can record the displacement by co relating these speckle patterns after a force is applied. Speckles are well defined on rough surface and displacement measurement can be more precise, if the speckles are well defined. Figure 1.11 below shows the schematic layout of digital laser microinterferometer based on speckle interferometry. The drawback of this system is that it needs a surface suitable to create a speckle pattern. Most of the MEMS device surfaces are made of either metals or silicon which reflects light. Primary requirement of speckle is to have rough surface where the surface instead of reflecting, scatters the light to form local interferences to create speckles. Thus it limits its range of usability in MEMS field.

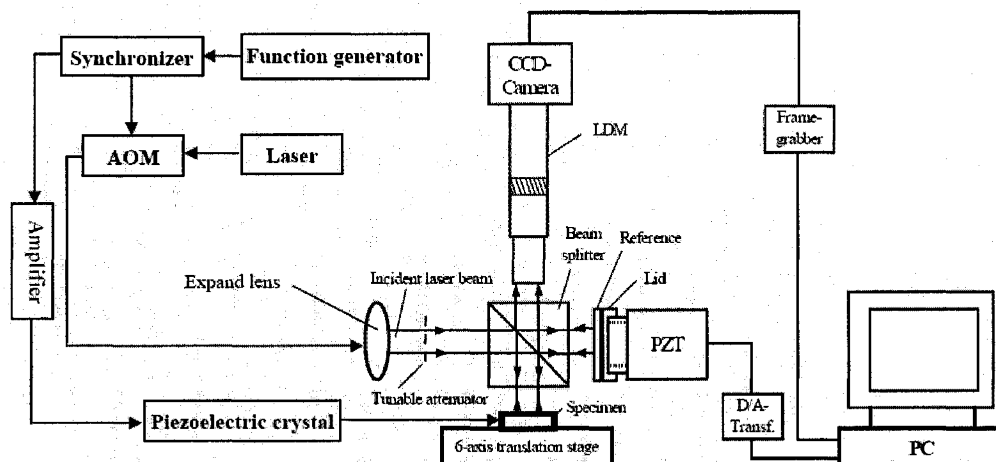

Figure 1.11 Schematic layout of digital laser microinterferometer [41]

1.20 Processing Techniques on a Fringe Pattern

The application of interferometric techniques in MEMS was made feasible only with the introduction of CCD camera and highly sensitive optical detectors. To detect surface and other information in macro structure holograms were used to record the information. Image processing was made easy after introducing the image processing programs using computers. To install a real time vision system in an interferometric technique a CCD camera connected to a frame grabber is used to capture static images of the interferogram. The CCD camera captures the images in pixels array where the intensity is recorded in their respective pixel. Since the intensity is recorded in an array, various processing techniques can be used to get the measured phase value of the interferogram.

1.21 Fringe Tracking

Until 1970 fringe tracking was the foremost method to analyze interferogram quantitatively [43]. It requires only one interferogram but was relatively imprecise. Fringe tracking works by recording the positions of the intensity maxima and minima, rest of the data is interpolated in order to create a phase map across a plane. Tilt direction between the references and test object should be known to determine the shape of the object, i.e. concave and convex as shown in Figure 1.12. Understanding a complicated surface profile like that of MEMS device using fringe tracking is impossible.

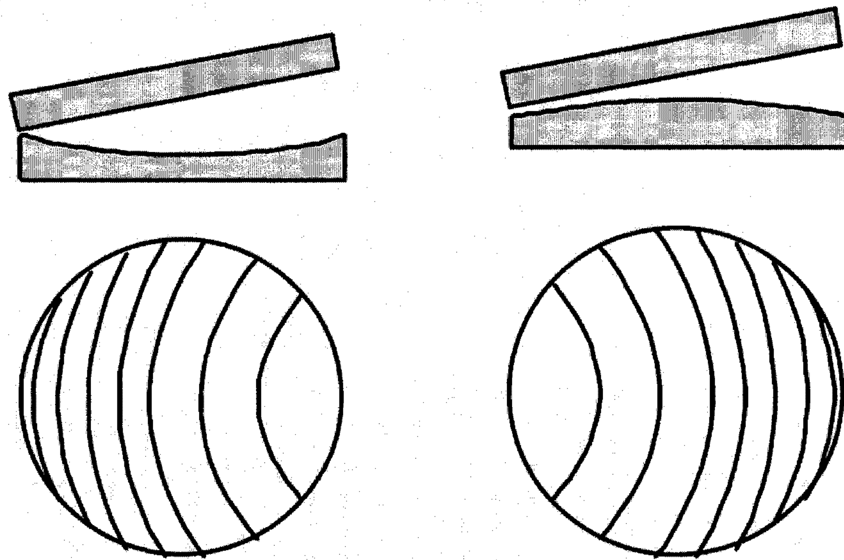

Figure 1.12 Fringe tracking method

1.22 Temporal Phase Measurement/Temporal Heterodyning

Temporal phase measurement introduces a known increment in the relative differences between the test and reference beams called phase shift. It is also called phase shifting method. From the phase shifting equation [45,46,47]

$$I_{(x,y)} = I_{0(x,y)}[1+V\cos\varphi(x,y)] \quad (1.3)$$

Where $I_{(x,y)}$ is the intensity of the interference pattern at the corresponding pixel of the CCD camera, $\varphi_{(x,y)}$ is the phase difference between the object and reference at that particular pixel, and V is the modulation of the fringes. This equation has three unknowns in I_0, V and φ. Therefore, a minimum of three phase-shifted images is required to find out the phase φ value of a particular point. Therefore at least three interferograms are necessary to process the phase measurement like as shown in Figure 1.13.

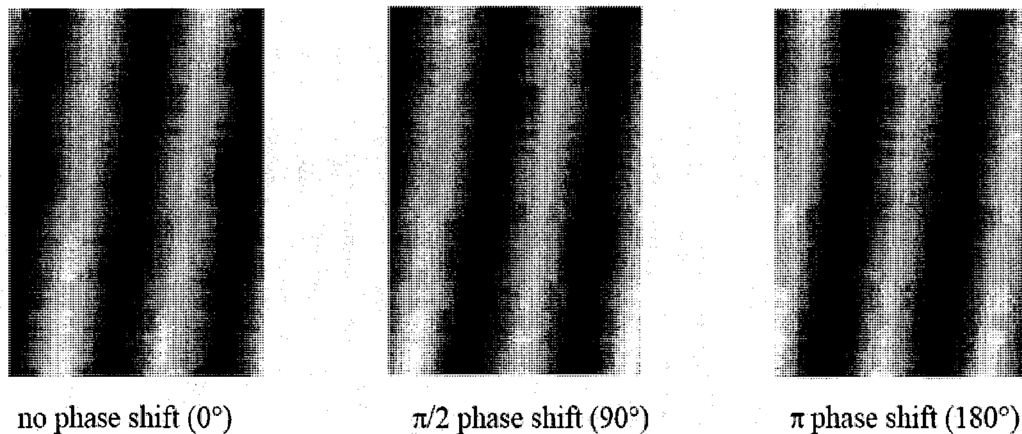

no phase shift (0°) $\pi/2$ phase shift (90°) π phase shift (180°)

Figure 1.13 Interferogram of different known phase shifts

The most common way to shift the phase is by changing the reference mirror in the optical axis. It is made possible by mounting the mirror on piezo stage which moves the mirror in nanometers. The measurement precision can be improved using more samples and using better algorithms [46,63]. The measurement can be precise with nanometer resolution with high repeatability. But temporal phase shifting methods are not most suitable for dynamic characterization. The setup to capture three or more interferograms instantaneously (also referred as spatial phase shifting) is possible only with multiple cameras, where alignment of cameras with pixel to pixel accuracy is complicated.

1.23 Fourier Transform

Fourier transform technique discretizes a single interferogram into three distinist spectral orders for a cosinusoidial function that represents the fringes. The number of fringes from the induced tilt between the references and test wavefront must be large enough to separate the spectral orders to enable filtering at the spatial frequency of the fringes. Inverse transform is then performed to phase encode the interferogram from arctangent function of the real and imaginary parts of the inverse transform [48,49]. A phase measurement from Fourier transform is more precise than fringe tracking but less than phase shifting. Its algorithms are much simpler and fast to process. Better filter to remove spatial noise improves the measurements [44]. The advantage of using Fourier transform over phase shifting (Temporal Phase measurement) and fringe tracking is given in Table 1.2 below.

Parameters	Fringe Tracking	Phase Shifting	Fourier Transform
Number of Interferograms	1	Minimum 3	1
Resolution	1 to 1/10 λ	1/10 to 1/100 λ	1/10 to 1/30 λ
Experimental effort	Low	High	Moderate
Sensitivity to external influences	Low	Moderate	Low
Cost	Low	High	Moderate

Table 1.2 Comparison of different fringe processing techniques

1.24 Objective and Scope of the Thesis

The primary objective of this research work is to develop a simple yet viable stroboscopic interferometer with a CW laser for comprehensive mechanical characterization of microstructures. The scope of the thesis includes

- Modeling and design of simple MEMS microstructures to study static and dynamic behaviors using the Raleigh-Ritz method.
- Designing and building Acousto Optic Modulated Stroboscopic Interferometer (AOMSI).
- Conduct experiments on various microstructures to characterize their surface, static, dynamic behavior.
- Comparing the experimental results with that of theoretical models to validate the design of the interferometer.

Chapter 2

Design and Modeling of MEMS device

2.1 Introduction

In microsystems, theoretical modeling and simulations play a vital role. Theoretical modeling [74,89] of MEMS devices involves understanding the microstructure when it is subjected to various electrostatic loads and boundary conditions. The modeling is done in order to understand the properties to predict their static and dynamic behaviors under different influences. For example, when these microstructures are activated with an electrostatic field, the structure deflects under the applied voltage. Similarly when the microstructure is made to vibrate, it resonates at a particular natural frequency to take the shape of the vibration mode. In our dynamic modeling natural frequency of the device and also the mode shape is simulated to understand the dynamic behavior.

2.2 Rayleigh-Ritz Method

Fundamental Frequency is of greatest interest when it comes to the analysis of vibration in a mechanical system. Rayleigh-Ritz improved the method with introduction of a series of the shape function multiplied by a constant co-efficient. The equation resolves to give better solution for natural frequency and mode shapes when a satisfying shape function is used for the geometric boundary conditions [50]. In the analysis for both static and dynamic behavior of the MEMS device the Rayleigh-Ritz energy method is used. In the

dynamic analysis of the cantilever the boundary characteristic orthogonal polynomials were employed and the same is adopted for the static deflection.

2.3 Energy Formulation

The energy formulation takes into account electro-mechanical influences. The thermal influences, however, are not considered in the model. Shown in Figure 2.1 is a schematic representation of a microcantilever with electrostatic and geometrical influences.

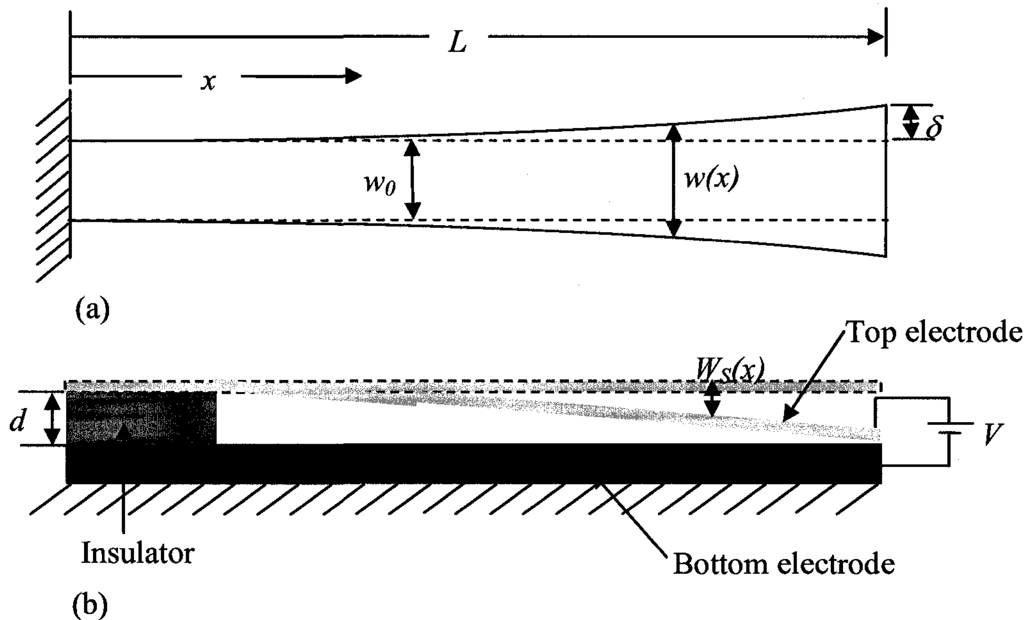

Figure 2.1 (a) Schematic top view of microcantilever width contouring (b) Schematic side view of an electrostatically actuated microcantilever

Where L is the length, x is the longitudinal coordinate, w(x) the positional width, w_0 the unconditioned width, d the dielectric gap (microcantilever-electrode spacing), V the applied voltage, and $W_S(x)$ the static deflection along the length of the microcantilever.

The electro-mechanical influences affecting a microcantilever are modeled with artificial springs as shown in Figure 2.2.

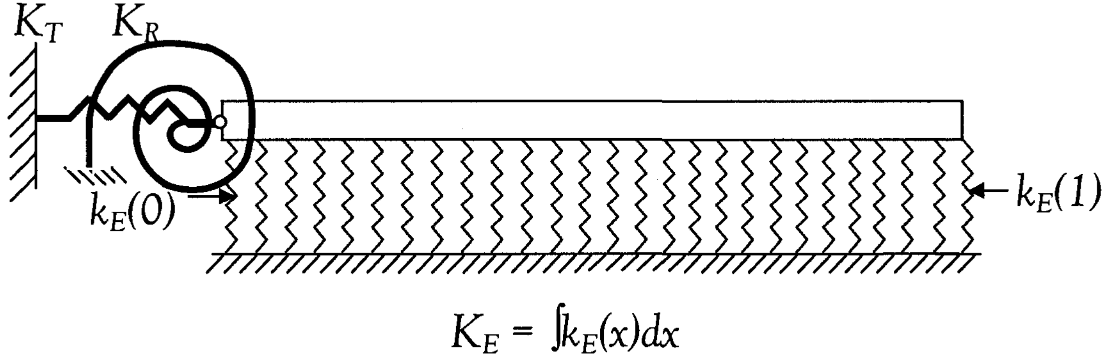

Figure 2.2 Equivalent microcantilever with artificial springs

2.4 Theoretical Formulation

The theoretical models for the static and dynamic analysis are introduced. The formulations are based on an energy approach in which the static and dynamic behaviour of the microstructure can be estimated by employing boundary characteristic orthogonal polynomials [50,51]. In the dynamic analysis the formulation becomes the classical Rayleigh-Ritz method, whereas in the static analysis a linearized non-homogeneous system is obtained for a given applied voltage.

2.5 Modeling the Static Behaviour

The static deflection W_S, is estimated from,

$$W_S(x) = \sum_{i=1}^{n} A_i^S \phi_i(x) \tag{2.1}$$

where the, A_i^S, are the static deflection coefficients of the beam, and ϕ_i, are the orthogonal polynomials, x, is a non-dimensional quantity equal to ξ / L and varies from 0 to 1, n is the total number of polynomials in the set. The strain energy of the beam is given by,

$$U_B = \frac{Eh^3 w}{24L^3} \int_0^1 \hat{F}(x)(W_S''(x))^2 dx \tag{2.2}$$

Where E is the elastic modulus, L is the length of the cantilever, w is the width, h is the thickness, $\hat{F}$ is a geometry conditioning function and W_S'' is the second derivative with respect to x. For the static analysis, the electrostatic potential energy is given by [22],

$$U_E = \frac{\varepsilon_r \varepsilon_0 L w V^2}{2d} \int_0^1 \hat{F}(x)\left(1 + \frac{W_S(x)}{d} + \left(\frac{W_S(x)}{d}\right)^2\right) dx \tag{2.3}$$

where third and higher order terms are ignored. Here, W_S is the static deflection for a given applied voltage V, ε_0 and ε_r are the permittivity of free space and relative permittivity of the dielectric medium, respectively, and d is the dielectric gap. In the case of an electrostatically actuated cantilever, the static equilibrium position is obtained from the condition,

$$\frac{\partial}{\partial A_i}[U_B + U_E] = 0 \tag{2.4}$$

The above equation results in the following linear system,

$$\sum_{j=1}^{n}\left[E_{ij}^{22} - V_1^* E_{ij}^{00}\right]A_j^S = V_2^* \int_0^1 \hat{F}(x)\phi_i(x)dx \tag{2.5}$$

$\forall i = 1...n$

where the following definitions apply,

$$E_{ij}^{22} = \int_0^1 \hat{F}(x)\phi_i''(x)\phi_j''(x)dx \tag{2.6}$$

$$E_{ij}^{00} = \int_0^1 \hat{F}(x)\phi_i(x)\phi_j(x)dx \tag{2.7}$$

$$V_1^* = \frac{\varepsilon_0\varepsilon_r wL^4V^2}{EId^3},\ V_2^* = \frac{\varepsilon_0\varepsilon_r wL^4V^2}{2EId^2}, I = \frac{wh^3}{12} \tag{2.8}$$

where I is the moment of inertia. One could obtain the static behaviour using Equation (2.5) for a given voltage. Static behaviour for various applied voltages on SOI MicraGem cantilever whose specification given below in Table 2.1 where calculated using the model described above.

Parameter Considered	**Values**
Length of the cantilevers (L)	810μm (measured)
Thickness (h)	10.5μm (measured)
Maximum width (w(x))	90μm (measured)
Dielectric gap(d_0)	~11μm (measured)
Young's modulus E	129.5 GPa (values given by the manufacturer)
Density ρ	2320kgm^{-3} (values given by the manufacturer)

Table 2.1 Specification of the SOI MicraGem Cantilever

The deflection was calculated for 15V, 29.5V and 55V and the magnitude of the deflection at the tip of the cantilever is tabulated below in Table 2.2 the characteristic shape of the deflected cantilever for the said voltages is shown in Figure 2.3.

Voltage	**Magnitude of Tip at 810μm deflection (nm)**
55V	377
29.5V	109
15V	27

Table 2.2 Theoretical tip deflection for static characterization

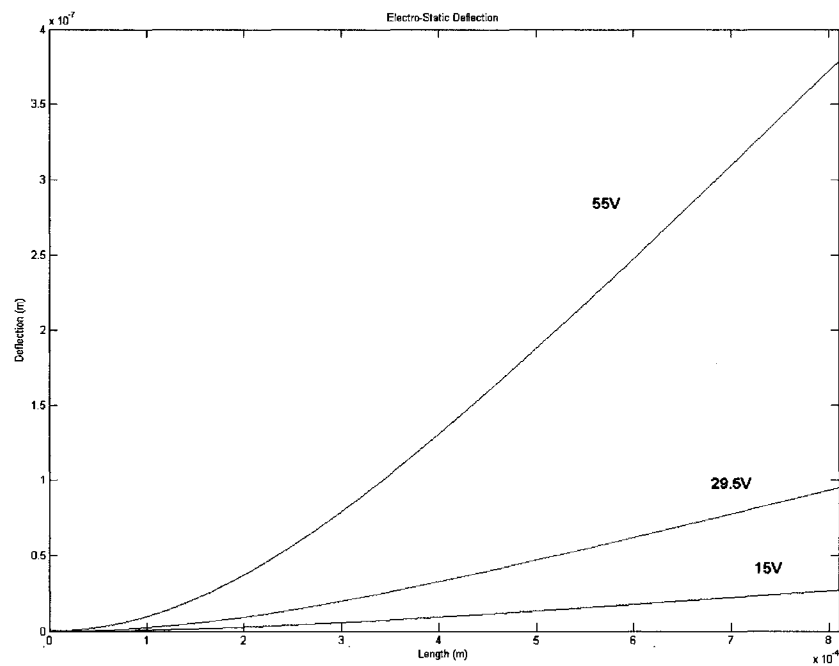

Figure 2.3 Static deflection

2.6 Modeling the Dynamic Behaviour

The estimation of the natural frequencies and mode shapes of the AFM cantilevers are carried out using the normal mode approach by applying boundary characteristic orthogonal polynomials in the Rayleigh-Ritz energy method [50]. This approximate numerical method is a simple way to analyze the flexural response of variety of structures such as beams and plates [51,52,54] and is employed here for this reason.

The assumed dynamic deflections W_D, of the cantilever beam are given by,

$$W_D(x) = \sum_{i=1}^{n} A_i^D \phi_i(x) \tag{2.9}$$

where A_i^D are the dynamic deflection coefficients of the beam. The natural frequencies ω_k (rad/s), of the system can be obtained by minimizing the Rayleigh quotient defined as,

$$\omega^2 = \frac{U_{MAX}}{T^*_{MAX}} \tag{2.10}$$

where U_{MAX}, is the maximum strain energy. In this analysis, the total strain energy of the cantilever system is given by,

$$U_{MAX} = U_B \tag{2.11}$$

where U_B is given by,

$$U_B = \frac{Eh^3 w}{24L^3} \int_0^1 \hat{F}(x)(W_D''(x))^2 \, dx \tag{2.12}$$

The maximum kinetic energy T_{MAX}, is defined by,

$$T_{MAX} = T_B = \omega^2 T^*_{MAX} \tag{2.13}$$

and is given by,

$$T_B = \frac{\omega^2 \rho h w L}{2} \int_0^1 \hat{F}(x)(W_D(x))^2 dx \tag{2.14}$$

where ρ is the material density. For the dynamic analysis, an artificial electrostatic stiffness per unit length is obtained from the static equilibrium position of the cantilever for a given applied voltage, and is given by

$$k_E(x) = \frac{\varepsilon_0 \varepsilon_r w L^4 V^2}{EI} \left[\frac{\hat{F}(x)}{(d - W_S(x))^3} \right] \tag{2.15}$$

The electrostatic potential energy for the dynamic analysis is then given by,

$$U_{ED} = \frac{1}{2} \int_0^1 k_E(x)(W_D(x))^2 dx \tag{2.16}$$

where W_S has been replaced by W_D for the dynamic analysis of the flexural deflection of the cantilever. Minimizing Equation (2.10) with respect to the deflection coefficients A_j^D, results in an eigensystem that uniquely characterizes the dynamic behaviour of the cantilever. The eigensystem obtained is given by,

$$\sum_{j=1}^{n} \left[E_{ij}^{22} - U_{ED} - \lambda_K{}^2 E_{ij}^{00} \right] A_j^D = 0 \tag{2.17}$$
$$\forall i = 1 \ldots n$$

Where the following definitions apply,

$$\lambda_K{}^2 = \frac{\omega_K{}^2 \rho \, h L^4}{E \, I} \tag{2.18}$$

Solution of Equation 2.17 will provide the natural frequencies and mode shapes for n number of modes. Dynamic behaviour for 1st and 2nd natural frequency of AFM cantilever whose specification given below in Table 2.3 was calculated using the model

described above. Shown in Table 2.4 are the calculated natural frequencies compared with that of the manufacturers' specification. Figure 2.4 shows the normalized 1st and 2nd mode shape obtained using the model.

Parameter Considered	Values
Length of the cantilevers (L)	350μm (measured)
Thickness (h)	1 μm (measured)
Maximum width (w(x))	35μm (measured)
Young's modulus *E*	169.5 GPa (values given by the manufacturer)
Density ρ	2330kgm^{-3} (values given by the manufacturer)

Table 2.3 Specification of AFM Cantilever

Mode	Natural frequency(simulated)	Natural frequency (by manufacturer)
1st	11.2 kHz	10.0 kHz ± ~3 kHz
2nd	70.4 kHz	n/a

Table 2.4 Theoretical Resonance Frequency

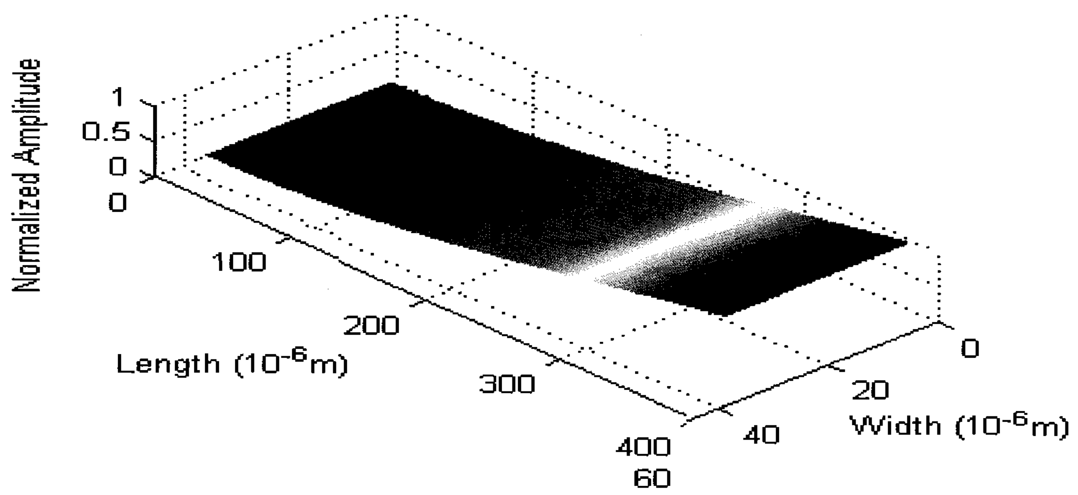

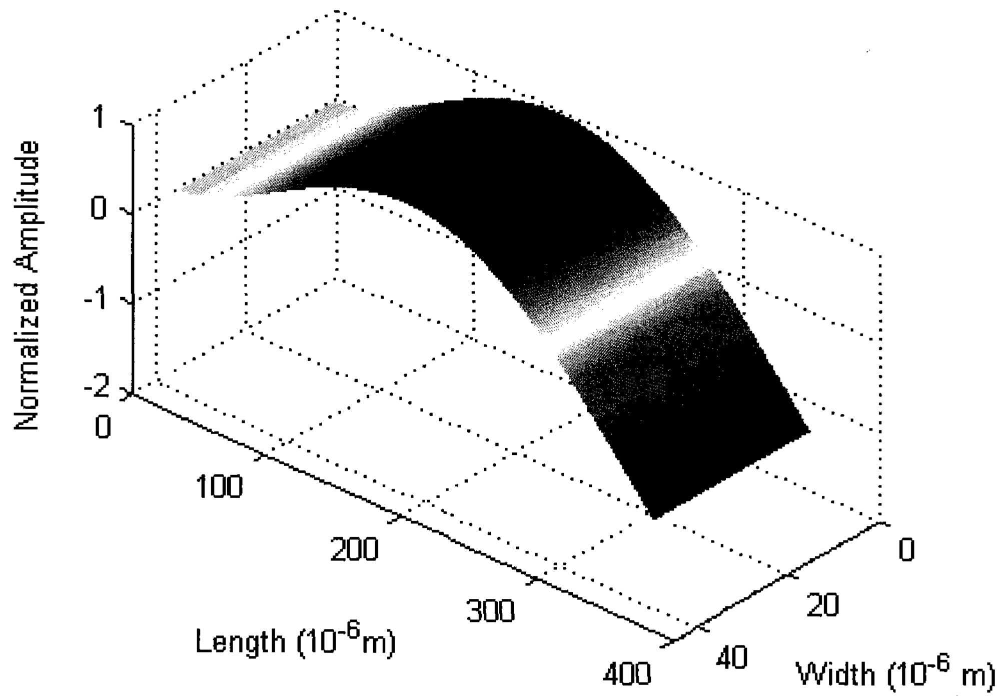

Figure 2.4 Analytical Representations of the 1st and 2nd Mode Shapes

2.7 Summary

Design and modeling of MEMS device is done to understand the electrostatic and mechanical influences for its static and dynamic behavior. The Rayleigh-Ritz energy method is implemented for the simulation. The results obtained from the theoretical model presented here were evaluated experimentally using the developed AOMSI and the comparisons are shown in chapters 5 and 6.

Chapter 3

Experimental Setup of Acousto Optic Modulated Stroboscopic Interferometer

3.1 Introduction

In this chapter the setup of the Acousto Optic Modulated Stroboscopic Interferometer developed for static and dynamic characterization of microdevices is detailed. Stroboscopy creates the illusion of slow-motion. In this regard, stroboscopy has been widely used in photography and also in industrial applications to freeze the motion of moving objects. The fundamental principle being that when the strobing frequency is equivalent to the frequency of the device in periodic motion, the motion appears frozen and is visualized in a still position. This strobing principle can be exploited in the freeze-frame visualization of high frequency cyclic motion [28] and hence, applied to high frequency resonating microstructures. Through the combination of a classical interferometer and a strobed monochromatic light source, measurement of in-plane and out-of-plane motions of microstructures is possible with resolution in the order of few nanometers. In the experimental method presented here, an AOM is used as the strobing module. This setup is the first of its kind to characterize the static, dynamic and surface profile characteristics of microstructures using on single equipment with a relatively simple design.

3.2 Basic Layout of the Interferometer

The optical setup of the Acousto Optic Modulated Stroboscopic Interferometer is shown in Figure 3.1. A 5mW, 632.8nm He-Ne laser source is directed into an AOM positioned at a Bragg angle (θ_B), of 0.7mrad with respect to the laser so as to maximize the efficiency of the first order diffraction. The AOM is excited at its center frequency of 85MHz, using a driver. A function generator is employed to modulate the AOM for strobing the laser at a desired frequency. When the crystal in the AOM is excited it creates an acoustic grating which splits the single incident laser beam into two optical outputs, the zero and the first order Bragg diffractions when the AOM is placed in the Bragg angle with respect to laser. Two $\lambda/10$ mirrors are used to widen the zeroth and first order diffractions. The zeroth order Bragg diffraction is terminated and the first order diffraction is then used for the experiments. The excitation is controlled with the TTL signal of the function generator which creates the time delay to modulate the first order diffraction beam which is used for measurements. A spatial filter is used to remove the spatial error in the optical path in order to obtain a smooth Gaussian beam profile [53,55]. The spatial filter employed here consists of a 10X objective lens, and 40μm pinhole and is used on the first order diffraction.

The interferometer configuration employed in the experimental setup is a Twyman-Green interferometer which consists of a polarizing beam-splitter cube, two quarter wave plates, and a reference mirror [29]. The advantage of using a Twyman-Green interferometer is the capability to control the intensity of the optical beam. In this aspect, the ability to control the optical intensity is important with regards to the material of the microstructure

being tested [45]. The polarizing beam-splitter divides the laser beam into two paths, one for the reference mirror and one for the microstructure and the quarter wave plates ensures the directional continuity of the optical path to the CCD camera [56,57]. Lens L1 is used to collimate the laser beam from the spatial filter. The collimated laser beam is passed through a lens pair of L2 and a microscope objective to define the field of view. Lens L3 is used for imaging the object onto the focal plane of the CCD camera which is connected to a data acquisition card. This module helps in transferring all the images captured in given time frame for further processing. A schematic overview of the layout is given in Figure. 3.1. A digital image of the experimental setup is shown in Figure. 3.2.

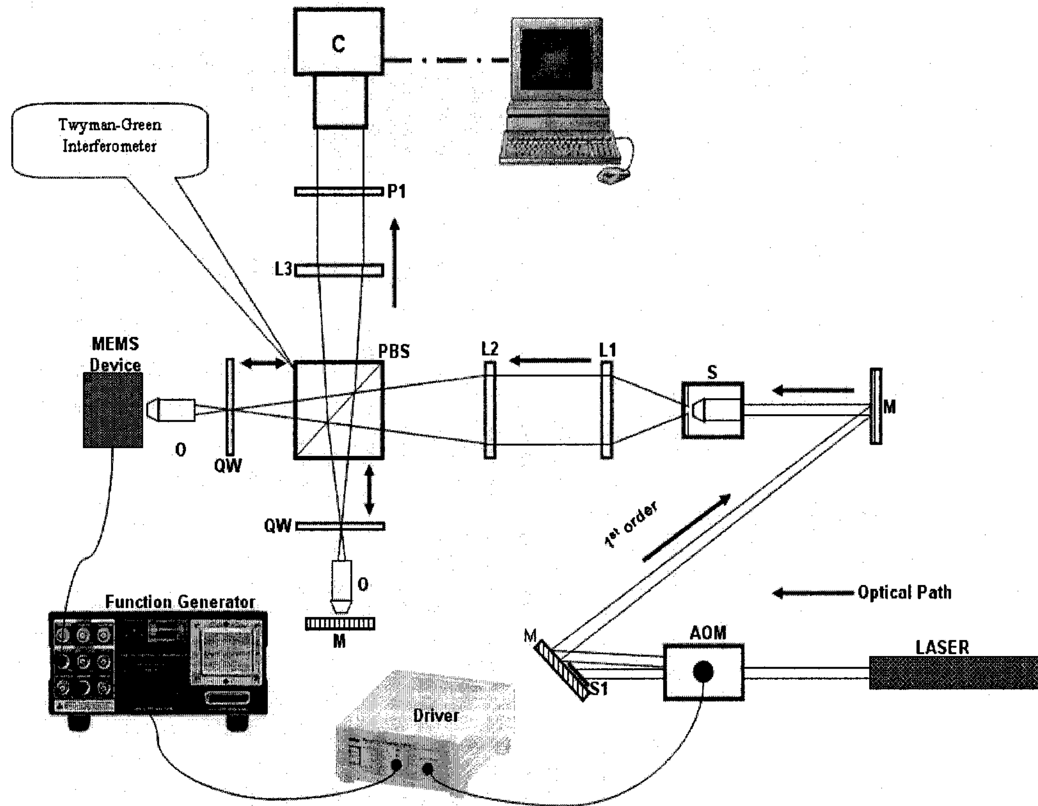

[M – Mirror; AOM – Acousto-Optic Modulator; S – Spatial Filter ; L1 – 100mm Collimating Lens ; L2 – 150mm Focusing Lens; O – 50mm Microscopic Objective; QW – Quarter Wave Plate; L3 – 300mm Imaging Lens; C – CCD camera; PBS –Polarized Beam Splitter, P1 – polarizer, S1 – Stopper]

Figure 3.1 Schematic overview of the principal components in AOMSI

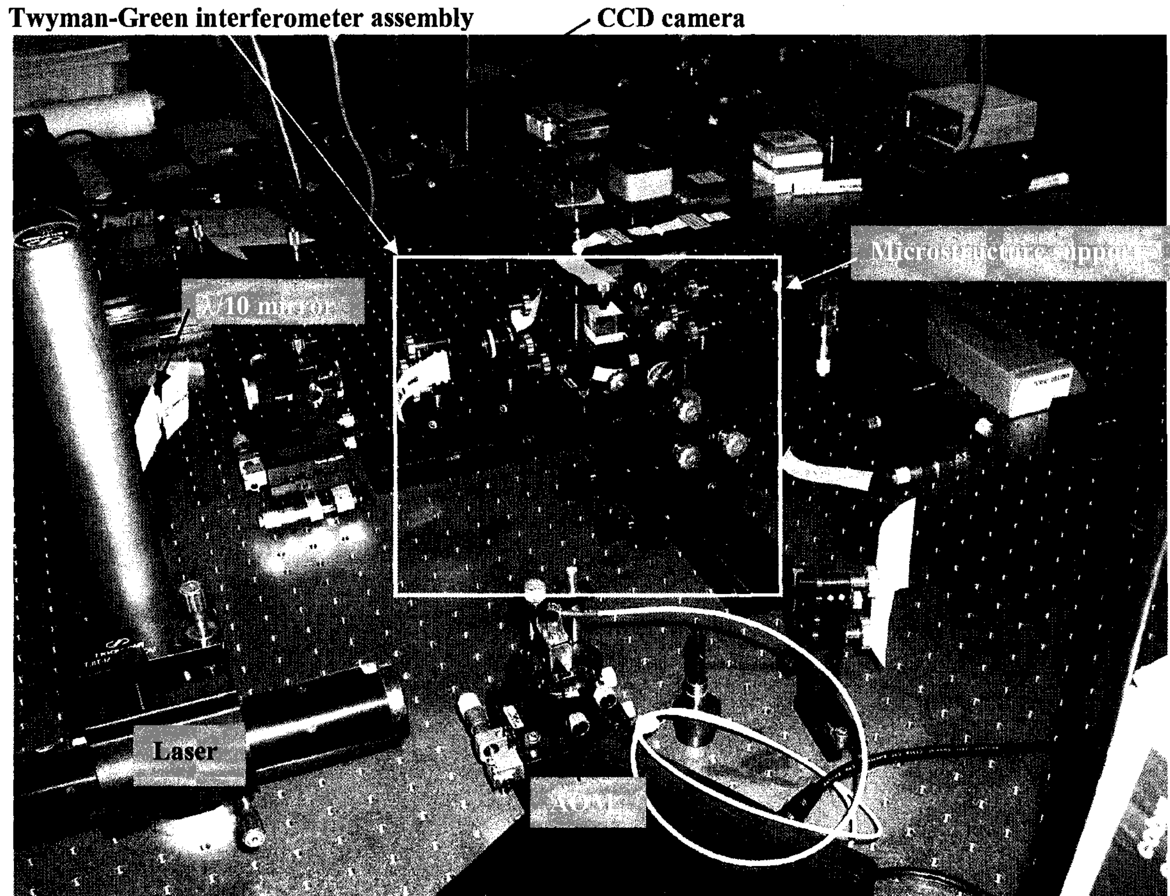

Figure 3.2 Digital image of the layout of the AOMSI assembly

3.3 Systematic Design and Alignment of the Optical System

The interferometer is built on a coherent optical path. The optical path needs to have extra attention in order to build a reliable setup of interferometer, therefore extra care should be given on every level of the setup to make sure that optical system is straight and aligned. Initially the He-Ne laser is mounted on a holder. The laser is aligned straight to a given reference. In the setup the mounting hole on the vibration isolation table is taken as reference to align the optical path and pinhole to align the height. The laser is

made to impinge on the AOM mounted on a stage that has 3 degrees of freedom to control the tilt, height and angle. This enables to properly align the crystal of the AOM with that of the incoming laser beam. The AOM is then connected to the output of the SMA (SubMiniature version A) connector of the RF driver using a 50 ohm impendence matched cable. The AOM is customized for an 0.5mm input beam with an active aperture of 0.8mm, that enables the laser to be directly passed on to the crystal without focusing. The AOM is adjusted to the Bragg angle of 0.7 mrad with respect to the laser [65]. When the laser beam intersects with the acoustic wave at the Bragg angle, there is first order and zero order beams getting diffracted from the AOM, as described earlier. Due to very small distances between the 0th and 1st order beams, two mirrors are used to increase the distance between them. The 0th order beam is then purged and the modulated 1st order beam is passed onto the spatial filter before being used for measurement.

Due to contaminants in the atmosphere the laser beam has spatial disturbances that can affect the accuracy of measurement. In order to filter these disturbances and to achieve uniform intensity, the measurement beam is spatially filtered. A spatial filter assembly consisting of an objective lens, pinhole, alignment system, and focusing axes can be used to remove the undesirable noise while transmitting most of the beam's energy. Here a 10X objective and $\phi 40\mu m$ pinhole is used to obtain a uniform beam output for our optical setup. The spatially filtered laser beam is collimated using a lens of 100mm focal length which increases the beam diameter to 4mm.

The collimated laser beam is passed through a lens pair of L_2 of 150mm focal length and a microscopic objective O of 50mm focal length placed 200mm apart. The object is placed on the focal plane of the objective lens to define the field of view. The reflected beams from the object pass through objective lens and Lens L_3 of 300mm focal length which images the object onto the CCD sensor. To get a sharp focus CCD sensor of the camera which is connected to a data acquisition card is positioned 300mm from Lens L_3. The CCD camera used in our system is progressive scan CCD with 648X492 active pixels with sensor size of 4.9X3.7mm.This optical arrangement gives us the field of view of 816X616 μm over the entire sensor and 1.1667μm per pixel.

3.4 Fringe Analysis using Fourier Transformation

In Fourier-transform method, intensity distribution I(x,y) of the interferogram is fitted with a linear combination of harmonic spatial functions[48].

$$I(x,y)=a(x,y)+b(x,y)\cos[\Phi(x,y) + 2\pi f_0 x] \quad (3.1)$$

where f_0 is the carrier frequency in the x-direction. Below in Figure 3.3(a) is the interferogram where the fringe is formed by two $\lambda/10$ mirror by the interferometer.

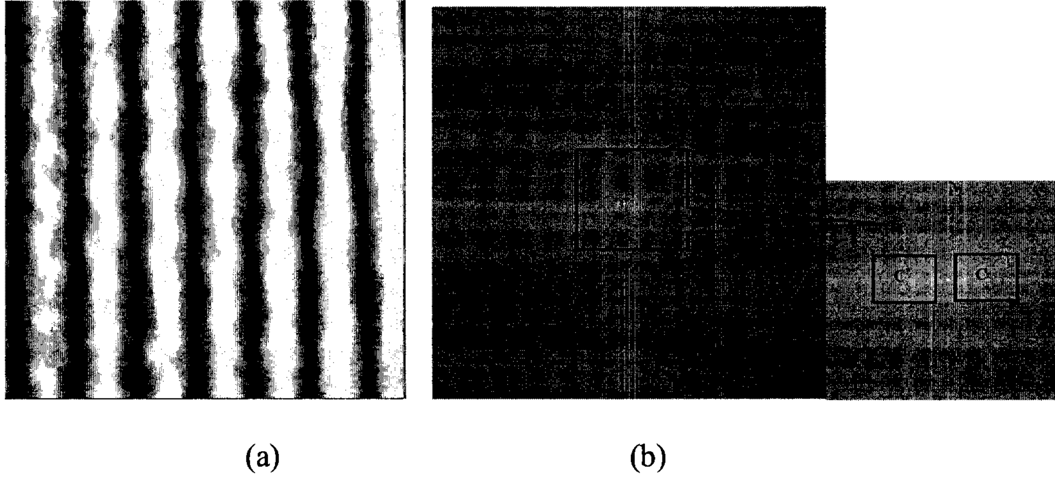

(a) (b)

Figure 3.3 (a) Interferogram (b) Spectrum image of the interferogram

The interferogram is then processed using FFT (Fast Fourier Transform) method to obtain the spatial frequency. The intensity is resolve into the equation below in the interferogram on each pixel.

$$I(x,y)=a(x,y)+c(x,y)+c^*(x,y) \tag{3.2}$$

Where $c(x,y)= ½.b(x,y).\ \exp[i\ \delta\ (x,y)]$ (3.3)

Here the symbol * denotes the complex conjugation and C is the complex Fourier amplitudes. The spectrum image above shows the both complex conjugation amplitudes of the interferogram in x- direction.

In the spectrum I(x,y) is a hermitean distribution in the spatial frequency domain. Using an adapted bandpass filter the unwanted additive disturbances can be eliminated together with the mode C or C^* as show in Figure 3.3(b). Performing an inverse Fourier transform on the filtered image gives the phase value calculated using Equation 3.4.

$$\delta_{(x\ y)}= \arctan\ [Im(C_{(x\ y)}/\ Re\ (C_{(x\ y)})] \tag{3.4}$$

Figure 3.4(a) below shows the band pass-filter and Figure 3.4(b) shows the result of inverse Fourier transform which gives a discontinuous phase image. The 2D line profile of the discontinuous phase image is shown in Figure 3.5. Taking into account the sign of the numerator and the denominator from Equation 3.4 the principal value of the arctan function having a continuous period of 2π is reconstructed.

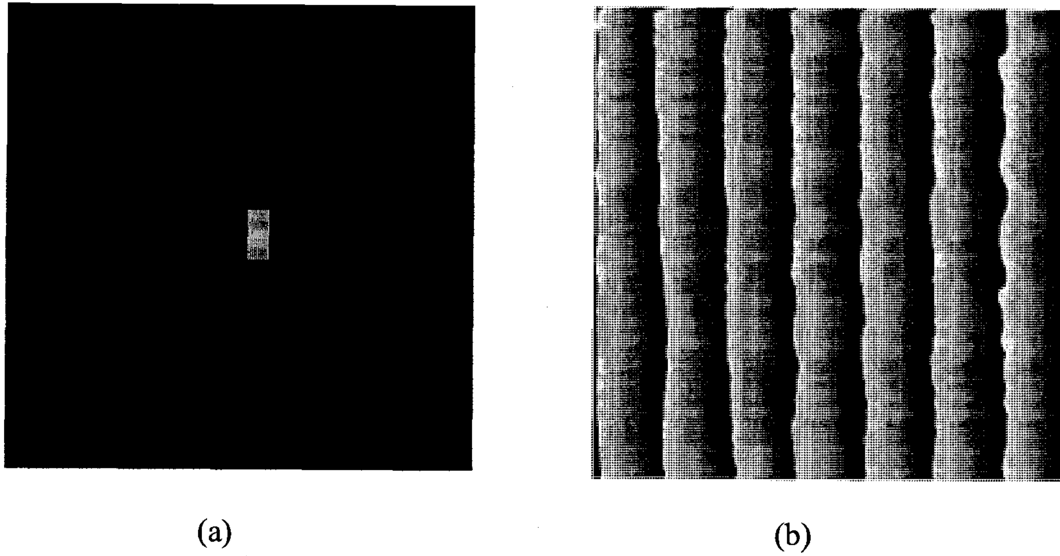

(a) (b)

Figure 3.4 (a) Band – pass filter mask (b) Inverse transform image of the interferogram

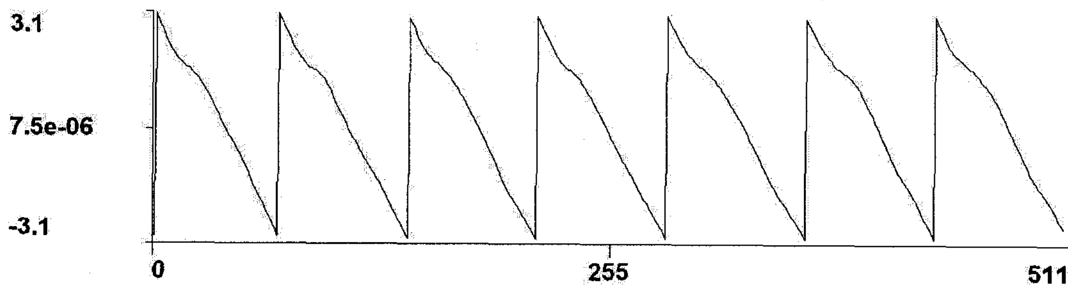

Figure 3.5 2D profile of the discontinuous image

The final step in fringe processing is to obtain a continuous phase from the wrapped mod 2π discontinuity. This process is called unwrapping where depending on the slope; a value of 2π is either added or subtracted along a line where phase jumps from 0 to 2π in order to obtain continuity. Figure 3.6 below shows 2D line profile of the continuous phase obtained from the discontinuous line profile in Figure 3.5.

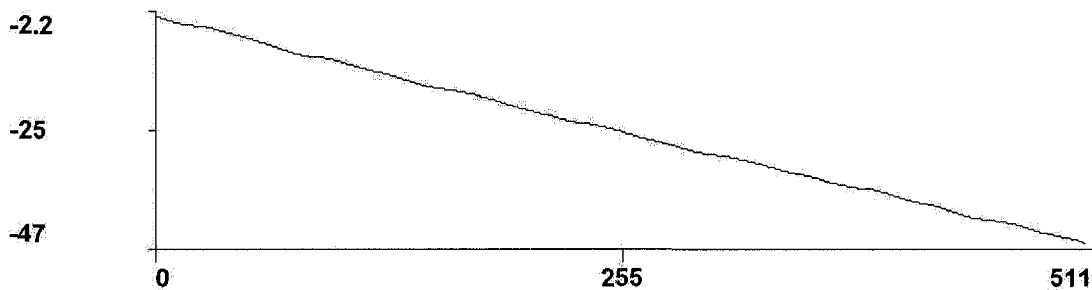

Figure 3.6 2D profile of the continuous profile

In the Figure 3.6 above, the X axis exhibits the field of view in pixels. The Y axis shows the displacement of the object in terms of unit less phase value that needs to be quantified in meters. A sensitivity analysis is done using two $\lambda/10$ mirrors to quantify this phase value which is discussed further.

3.5 Sensitivity Analysis

To identify sensitivity, a $\lambda/10$ mirror is used as an object. Since the reference mirror is in line with the camera the new object mirror is adjusted to get straight fringes on the camera. Obtaining straight line fringes in any direction proves that the optical setup is prefect and the optical path of the interferometer is giving planar wave fringes. With this we change the angle of the object mirror and capture images with different number of fringes to calculate the sensitivity of the system. The field of view, as discussed earlier, for each pixel is calculated to get the distances between the fringes. In planar wave

interference, the distances between the fringes depend on the wavelength of the interfering beams and the half angle between them as shown Figure 3.7. The angle of the interfering beam can be calculated using the following Equation 3.5.

$$d = \lambda / 2\sin(\theta / 2) \tag{3.5}$$

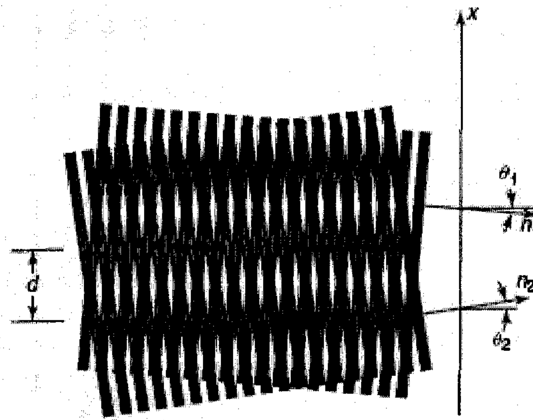

Figure 3.7 Planar wave interference, $\theta_1 = \theta_2 = \theta / 2$ (in Eq: 3.5)[95]

Where d is the distance between the fringes and λ is the wavelength of the light source and θ is the angle of interference. The fringes were analyzed using Fourier transform function of the FringeProcessor™ software [104]. The output of the Fourier transform for out-of-plane displacement is a unit less phase value. In order to correlate this unit less phase value to a measurement of displacement in width dimensions, sensitivity is required. To identify the sensitivity the out-of-plane displacement calculated knowing the field of view and the angle of interference between the two mirrors at different angles, as shown in Figure 3.8.

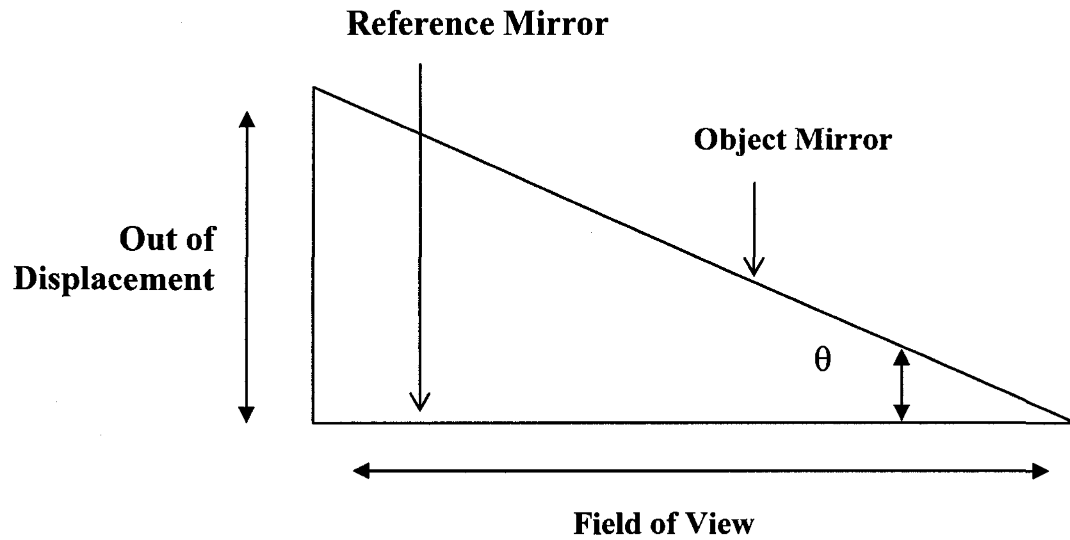

Figure 3.8 Angle between reference mirror and object mirror

When there is change in the angle, the fringe formation is altered in the image. For each and every angle a respective interferogram was captured and analyzed using FringeProcessor™. The experiments done with different number of fringes and their corresponding displacements are shown in Table 3.1.

# of Fringes	Interference Angle (rad)	Out of plane displacement (M)	Phase Value
1	0.0335	3.64E-07	6.27
2	0.0535	5.81E-07	12.53
5	0.08	8.68E-07	18.55
7	0.1195	1.26E-06	31.38
9	0.1675	1.82E-06	43.88
10	0.199	2.16E-06	50.16
14	0.2815	3.06E-06	68.98
16	0.339	3.68E-06	75.26
19	0.3925	4.28E-06	94.05

Table 3.1 Tabulation of number of fringes to out of plane displacement

The out-of-plane of displacement was plotted against the unit-less phase value in the Figure 3.9 to calculate the sensitivity factor.

The sensitivity factor can also be theoretically calculated using Equation 3.6.

$$h = \frac{\lambda \Phi}{2\pi(Cos\phi_1 + Cos\phi_2)} \qquad (3.6)$$

where Φ is the phase value, λ is the wavelength, θ_1 and θ_2 are the angle of incidence and angle of reflectance of the laser beam with respect to object normal. For designed optical system the $\phi_1 = \phi_2 = 0$ which reduces the Equation 3.6[61] to

$$h = \lambda \Phi / 4\pi \qquad (3.7)$$

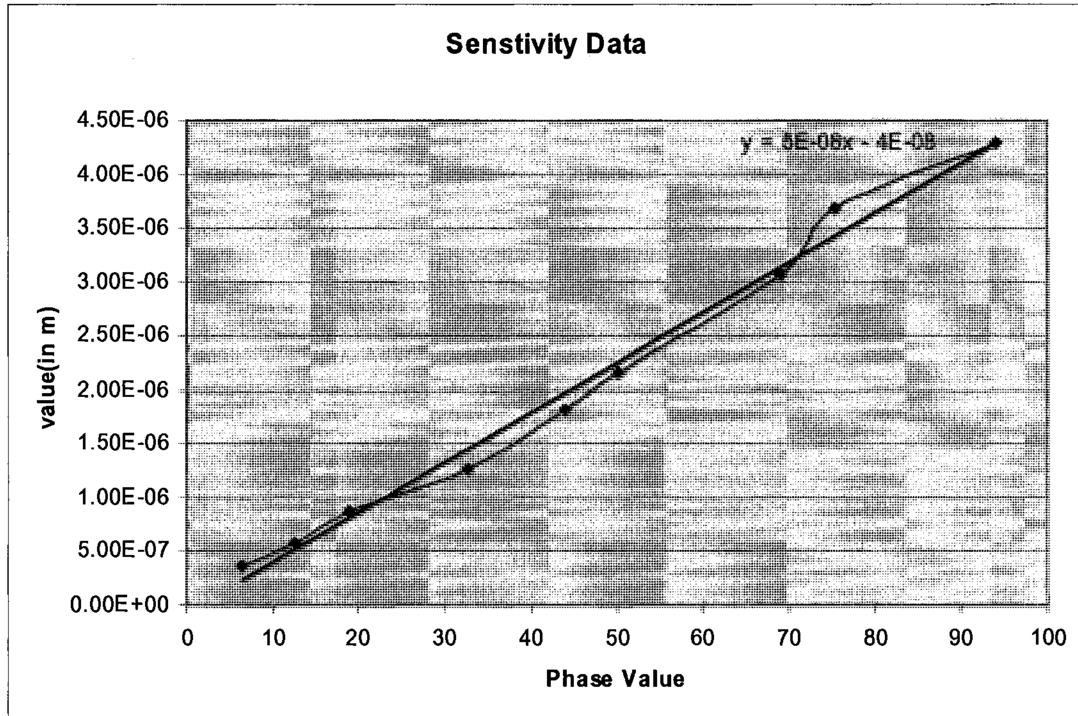

Figure 3.9 Sensitivity Data of the System

The slope of the line gives the sensitivity factor as 50nm which matches with the theoretical value for 632.8nm which is 50.38nm using Equation 3.7. Sensitivity analysis is investigated to understand the sensitivity of the system in addition to the error caused in post processing, which is due the background intensity in the interferogram. Varying the number the fringes also causes the object to move away from the focus. Therefore a optimal number of fringes is required for experimental work.

3.5 Optimization of Measurement Method

The post processing of the interferograms not only provides us with the out-of-plane displacement but also the surface information in the form of average surface roughness

(R_a) with suitable filters. R_a represents the noise level in the system which get reduced when the number of fringes are at 8 to10 .The graph in Figure 3.10 shows the value of the R_a for various numbers of fringes.

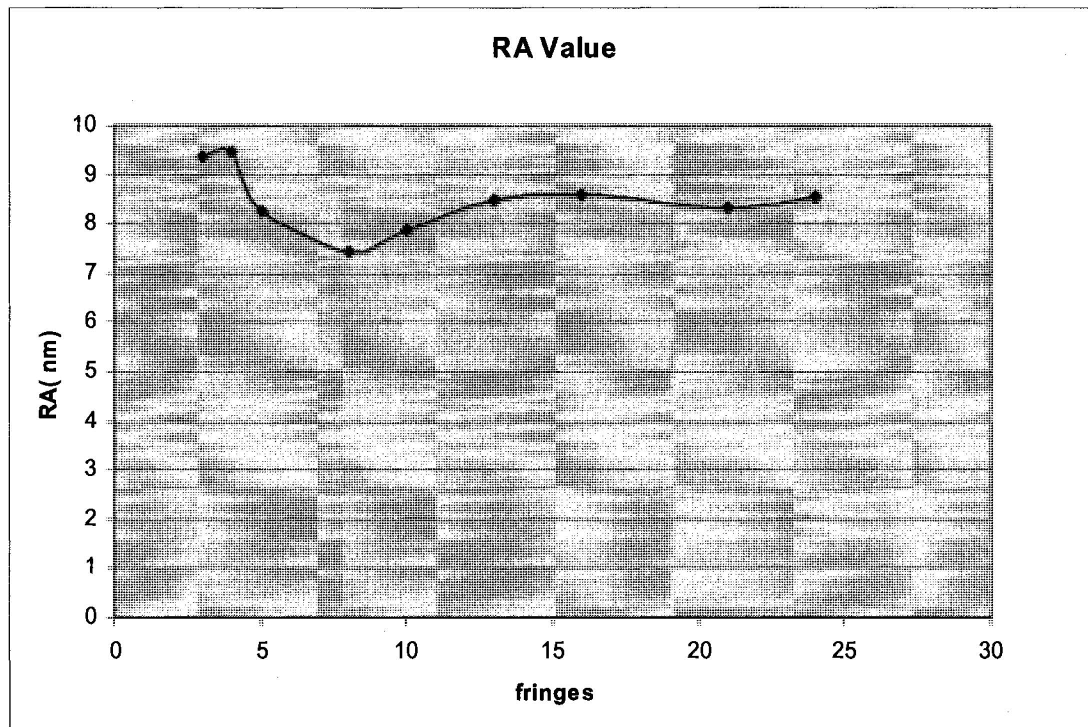

Figure 3.10 Ra Value of the micro mirror for various number fringes.

From the graph it is concluded that to get better surface information it is better to opt for 8-10 fringes. Ideally if there is less number of fringes, the depth of focus would be optimum. But fringe processing using Fourier transformation which requires more number of fringes; however tilting the object to obtain more fringes will move the object away from the depth of focus of the optical arrangement, which is clearly indicated in the graphs.

3.4 Summary

An optical setup is done on a vibration isolated table as per the schematic layout done for AOMSI. Instrumentation required for surface profiling, static and dynamic behaviors are implemented. The camera is connected for real time vision and for capturing static images. Sensitivity analysis of the tool was carried out and optimization of measurement methodology was established. The sensitivity factor of the optimized measurement methodology was found to be in good agreement with reported results.

Chapter 4

Surface Metrology and Static Characterization

4.1 Introduction

In the development of microstructure devices, there is a significant focus in the surface information of the microstructures. Currently, surface profile is studied using scanning electron microscope (SEM) or AFM. However there are various constraints on resolution and the types of materials that can be tested [58, 59]. Considering the limitations of these instruments, which are also expensive, an interferometric optical method [103] can be a versatile solution. AOMSI is one such instrument designed to give surface information of the structure in nanometer resolution and static deflections for different loads. It can be used on any type of material that has a minimum reflectivity around 30%. Presented in this chapter are the experimental details of surface metrology conducted on a micro-mirror and low frequency static characterization on micro-cantilever.

4.1 Surface Metrology

A sample surface metrology is presented using a torsional micro-mirror fabricated using the MicraGeM SOI fabrication process. The surface area of the mirror is 250 x 250μm^2. Given in Figure 4.1 is an SEM image of the torsional micro-mirror.

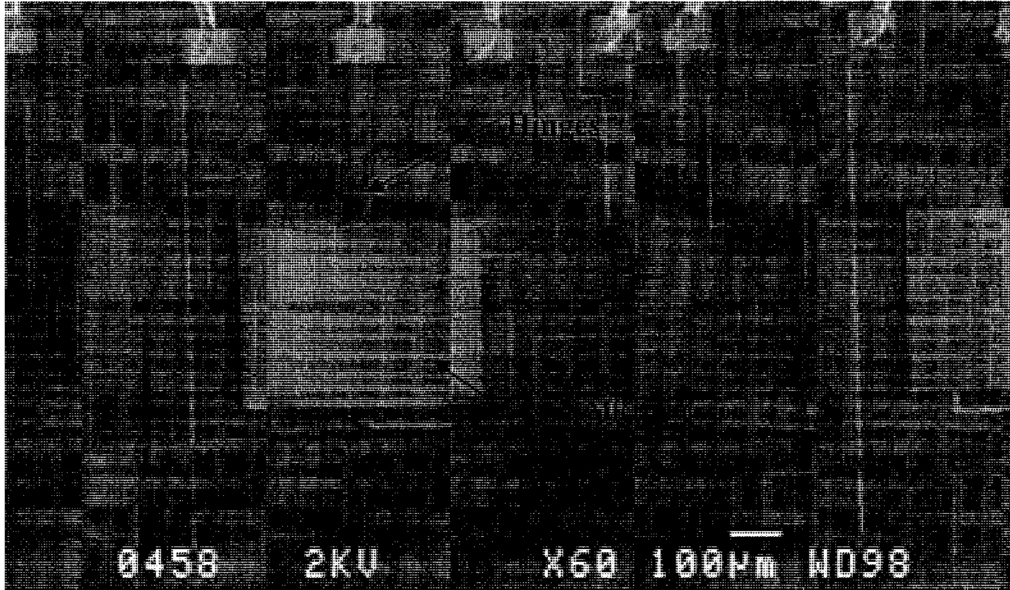

Figure.4.1. Torsional scanning micro-mirror fabricated using MicraGeM SOI technology.

In the experimental setup, a single CCD camera was employed; hence, it was possible to capture only a single interferogram at one time. The main focus in fringe processing is to calculate the phase information of the interferograms and the most widely used methods in optical metrology for fringe processing are either Fourier transformation [44] or phase shifting methods [45]. Since this interferometer is generally better suited for dynamic measurements, it is not possible to employ temporal phase shifting. Hence Fourier transformation was employed in order to obtain the phase information. Shown in Figure 4.2 is a torsional micro-mirror with a characteristic fringe pattern obtained with the AOMSI.

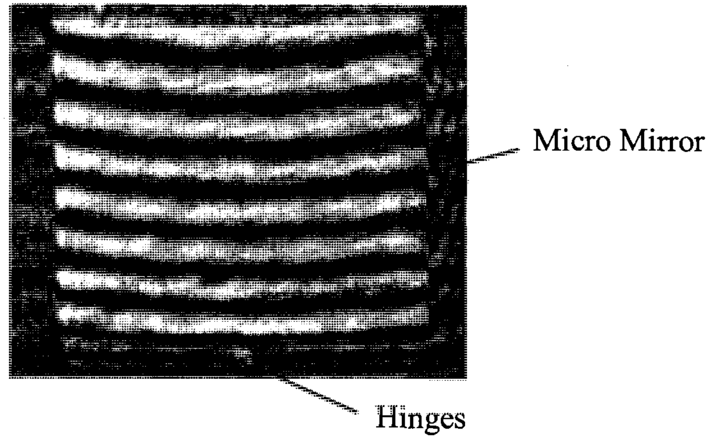

Figure 4.2 Fringe pattern from surface of the torsional micro-mirror.

The Fringe pattern is analyzed using the Fourier transform method with Fringreprocessor™ software and the wrapped phase value of the image is obtained, Figure 4.3. Subsequent unwrapping and conversion of phase to height values using Equation 3.3, provides us with the topography and out-of-plane displacement in Figure 4.4.

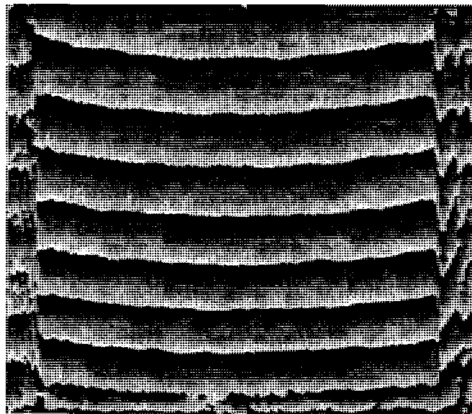

Figure 4.3 Wrapped image after the inverse analysis of the Fourier transform method

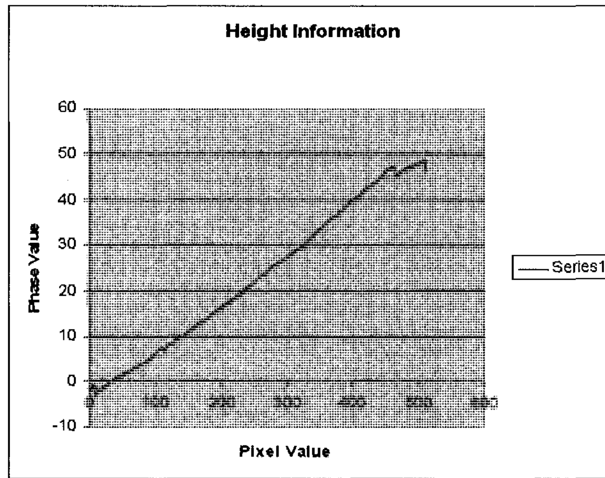

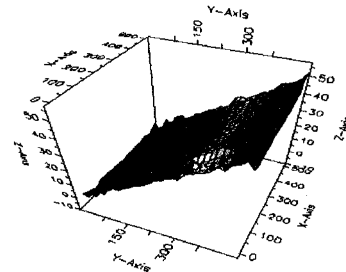

2D 3D

Figure 4.4 2D and 3D information of the micro-mirror with the tilt information

A least squares fit was carried out on the unwrapped phase image to remove the tilt from which the surface information is obtained with a resolution of ~10nm. Figures 4.5 and 4.6 represent the surface information obtained for the torsional micro-mirror in 2D and 3D. The micro-mirror tested shows stress formation on the surface [88,11,86].

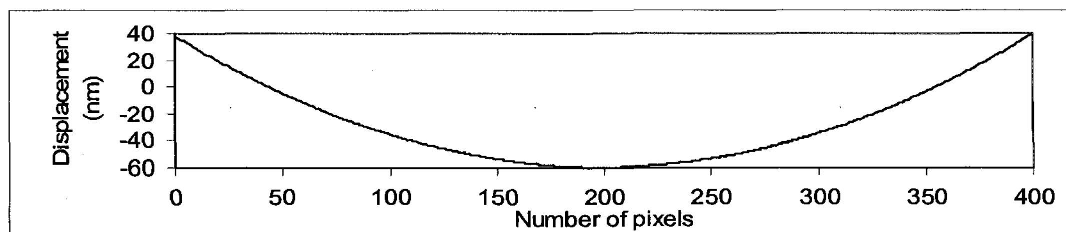

Figure 4.5 2D Profile of the surface of the torsional micro-mirror.

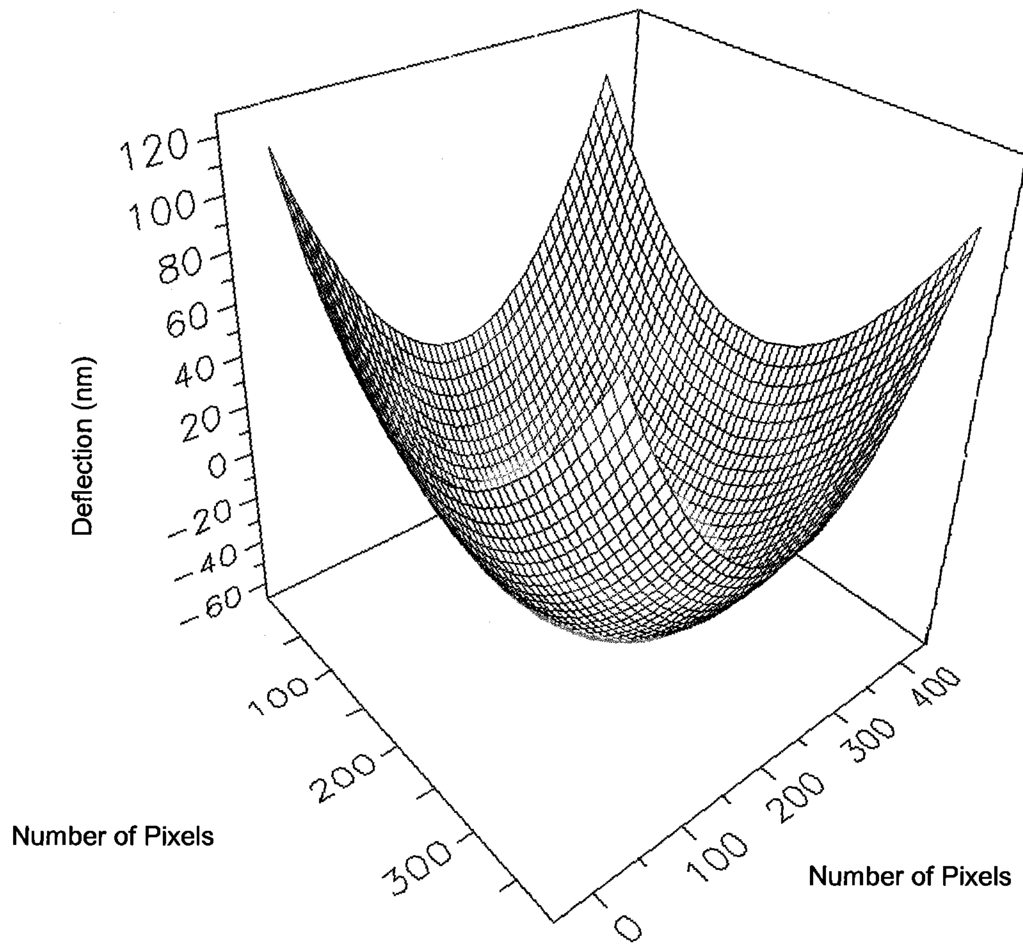

Figure 4.6 Surface characteristics obtained for the SOI torsional micro-mirror. The curvature and edge deflections are indicators of stress concentrations

4.2 Surface Metrology on a Connecting Pads

The experimental results show the ability of AOMSI to measure the surface profile of a micro-mirror with nanometer resolution. In order to understand the ability of AOMSI to characterize devices other than regular mirrors that have depth information, experiments

were conducted on connecting pads on a MEMS loose die. Figure 4.7 shows the interferogram and surface information of MEMS loose die along with the pads taken into consideration.

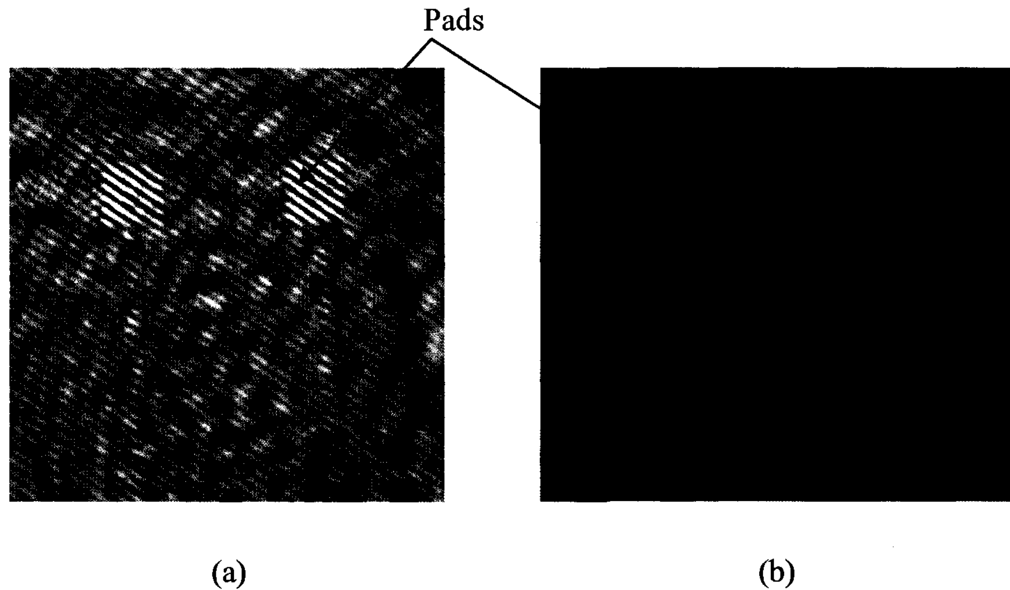

Figure 4.7 (a) Interferogram (b) Surface information of the surface

4.3 Importance of Static Characterization

MEMS are unique in their integration of electronics and mechanical components within the design architecture. In this context, intrinsic factors such as mechanical, electrical and material properties, affecting the performances of MEMS devices, need to be investigated in order to quantify their combined effect on the static behavior of the microsystem. In this regard, low frequency static applications, where the repeatability of the motion after a given time period, include torsional micro-mirrors, micro-switches and other micro-active-components. These types of devices can be said to operate in a quasi-

static state due to the surface motions of these types of micro-devices being much lower than the natural frequency of the device. Hence, on its own, the analytical model can only serve to estimate the operational characteristics of the MEMS device, therefore, experimental testing is needed to augment and complement the theoretical model [87]. In order to obtain accurate data, specially designed testing methods for microscale devices are needed [86,74].

In many applications electrostatically actuated MEMS are subjected to dynamic excitation frequencies well below the natural frequencies of the device. For example, pressure sensors and scanning mirrors applications require movement of the flexible structure at frequencies well below the natural frequencies. It can be safely assumed that at very low frequencies, well below the natural frequencies, the dynamic effects are negligible. Consider a MEMS device, as shown in Figure 4.8, in which an electrostatically actuated device is subjected to an external dynamic excitation. In Figure 4.8 the MEMS microcantilever structure is actuated with an applied piezo-electric mechanical excitation, and an applied *DC* voltage modeled with artificial electrostatic spring's k_E. In applications where electrostatically actuated MEMS structures are used at low frequencies, it is important to estimate the behavior of the MEMS structure at these low excitation frequencies. Even though, the behavior of the structure is close to being static behavior at very low frequencies, it is important to measure the deflection at lower excitation frequencies.

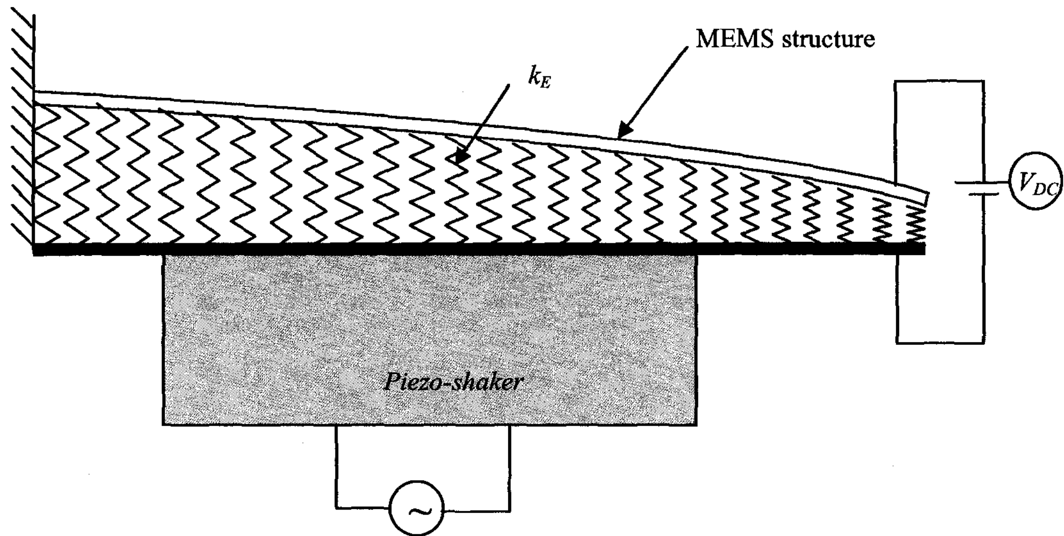

Figure 4.8 Low frequency excitation using a piezo-stack. Applied electrostatic potential is modeled with artificial springs k_E

This necessitates a method that can measure the static deflection under very low frequency excitation. Here it proposes an AOMSI based method to measure the static behavior under low frequency excitation. By tuning the AOM frequencies close to the excitation frequency, one can measure clearly the deflection. An experiment without strobing facility would not be able to measure this static behavior.

One of the principal factors to consider is how to perform direct measurements on MEMS devices in a way that is indicative of the actual micromechanical elements used in the microsystem. However, due to the micron-scale of MEMS devices, the method used for the testing must be carefully considered because of the difficulties in directly measuring forces and other influences at the micro-level. In this regard, the elastic property

governing the mechanical qualities of the microsystem, for a given operational environment, can be deduced through the response of the system to an applied load [83,6].

A non-contact interferometric optical instrument is a versatile solution for the testing of the static deflection of MEMS structures. Measurements of surface profiles of MEMS components are currently achieved by two main techniques, probing methods [5,4] and optical nondestructive methods [32,85]. Optical methods are advantageous over probe-based techniques as optical methods are of high speed, non-contact and are capable of providing full-field results with high spatial resolution [85]. AOMSI is one such instrument designed to give static surface information and dynamic mode shapes with nanometer resolution.

In this work, the low frequency static deflection of a MicraGeM technology SOI cantilever [105] to an applied electrostatic potential is investigated using the AOMSI approach.

4.4 AOMSI for Low Frequency Static Characterization

The important capability of stroboscopic interferometry compared to other characterization tools is that it gives a static image of the device through an interferogram obtained even when the device is in the dynamic state. Interferogram images can be used to predict the elastic properties of the device more precisely. An overview of the process is shown in Figure.4.9.

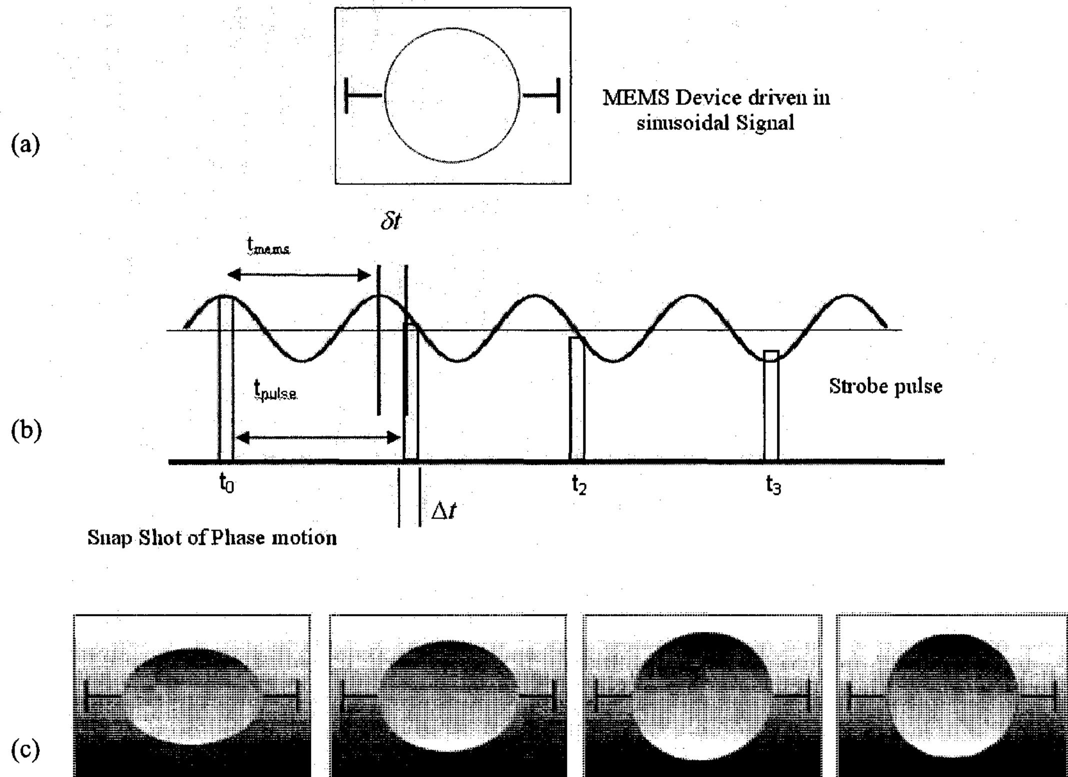

(a) Surface of MEMS Structure. (b) Driving Frequency and Strobe Frequency. (c) Surface Capture of the Structure for Various Freeze-Frames.

Figure 4.9 Methodology for static characterization of vibrating microstructure

In Figure 4.9b, the driving signal for the MEMS device t_{mems}, is triggered at the same time as the strobing signal t_{pulse}, Δt is the time delay applied to the strobing signal in order to capture the surface image with the CCD camera at a position along the dynamic state that is of interest as shown in Figure 4.9c.

With ω as the frequency at which the device is driven, it is assumed that,

$$\omega = 2\pi / t_{mems} \tag{4.1}$$

In order to obtain static images, the following condition is required

$$t_{pulse} = t_{mems} \tag{4.2}$$

therefore,

$$t_{pulse} = 2\pi / \omega \tag{4.3}$$

4.5 Measurement of Static Deflections

Shown in Figure 4.11 is a scanning electron microscope (SEM) image of a MicraGeM SOI technology cantilever array. In this figure, the length of the cantilevers is 810μm, the thickness was measured as 10.5μm, and the maximum width is 90μm as shown in Figure 4.10. The measured dielectric gap was ~11μm. One cantilever was tested device under test (DUT) at 15V, 29.5V and 55V, respectively. The DUT with fringes at 15V, 29.5V and 55V that were used for computing the deflections are shown in Figure 4.12. In the theoretical analysis, Young's modulus E was taken as 129.5 GPa, and the density as 2320kgm^{-3} (values given by the manufacturer).

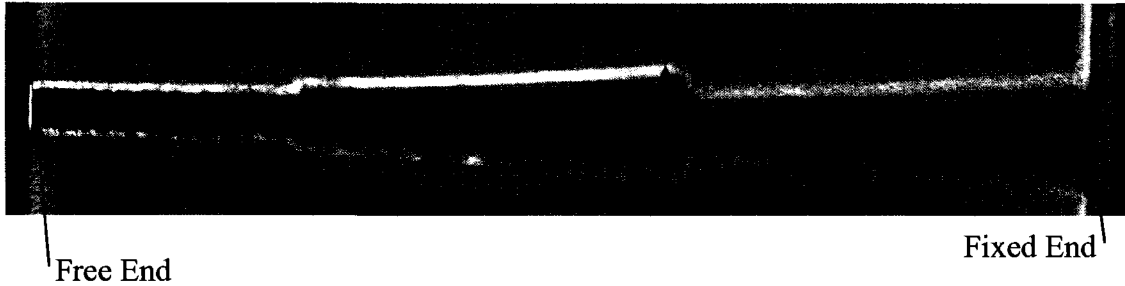

Figure 4.10 Microscopic image of the micragem SOI technology cantilever used for static deflection experiment.

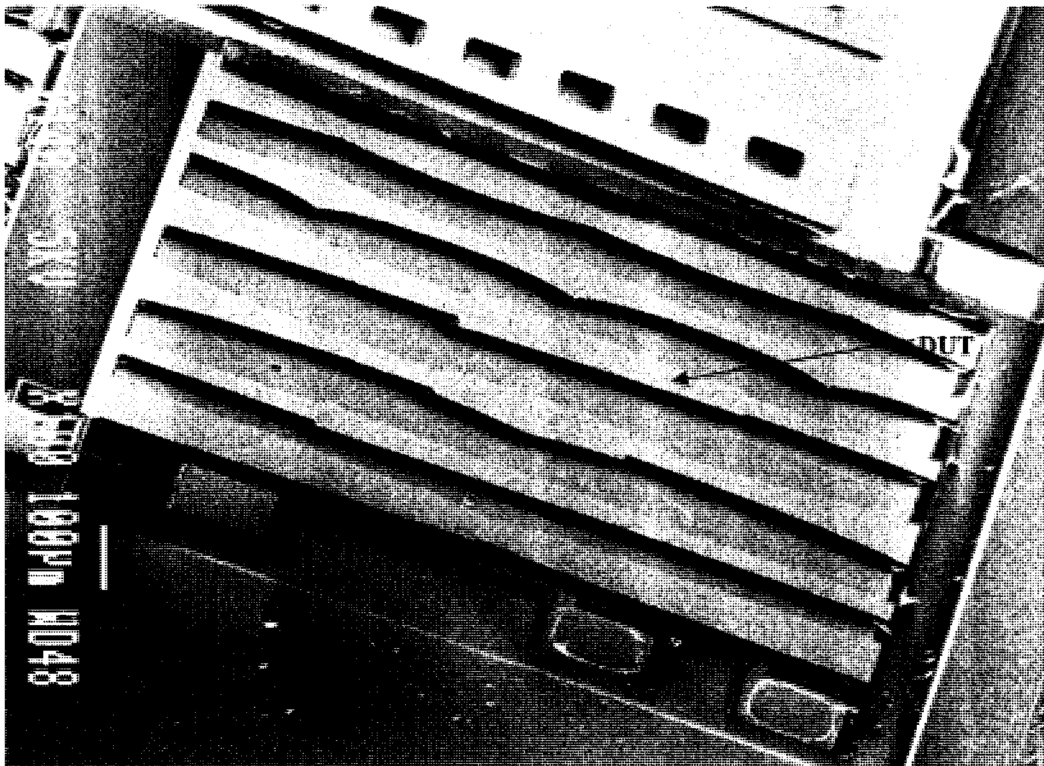

Figure 4.11 An SEM image of an SOI MicraGem technology cantilever array

As described earlier, a 30Hz progressive scan CCD camera with 648 x 492 pixels is used to capture the interferogram. The setup allows one to view the microstructure and to

evaluate the behavior in real time. Shown in Figure 4.12 are the interference fringes as seen on SOI MicraGeM cantilever actuated at various static DC voltages.

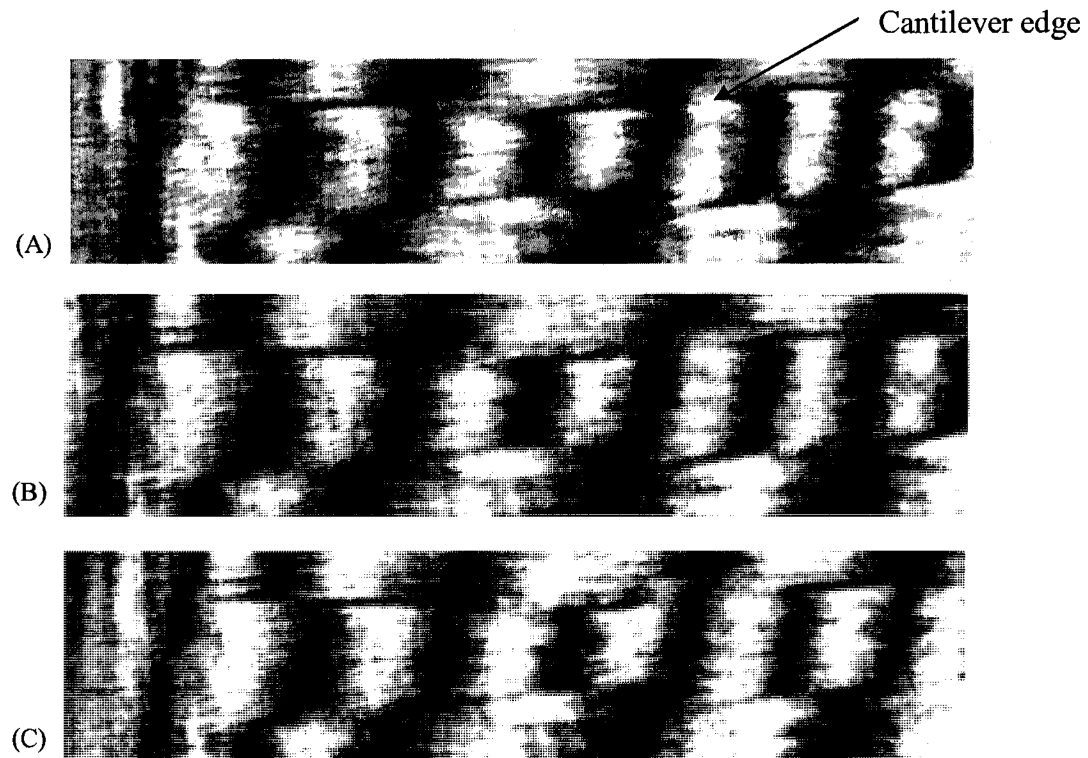

Figure 4.12 Fringe patterns obtained for the DUT at various voltages. (a) 15V. (b) 29.5V. (c) 55V.

For the characterization of static deflection, the fringe pattern was obtained after strobing at the same frequency as the excitation (the device was excited at 5% of its natural frequency). Processing the interferogram as described in described earlier using Fourier transformation and subsequent filtering, deflection of DUT at various static voltages was obtained. Shown in Figure.4.13 is the deflections of DUT for three different static voltages obtained experimentally compared with the theoretical deflection obtained

analytically, using Raleigh-Ritz approach as discussed in Chapter 2. For the experimental graphics the size of each pixel corresponds to length of 1.1667μm as discussed in chapter 3 so that the 350 pixels seen correspond to 410μm seen on the cantilever.

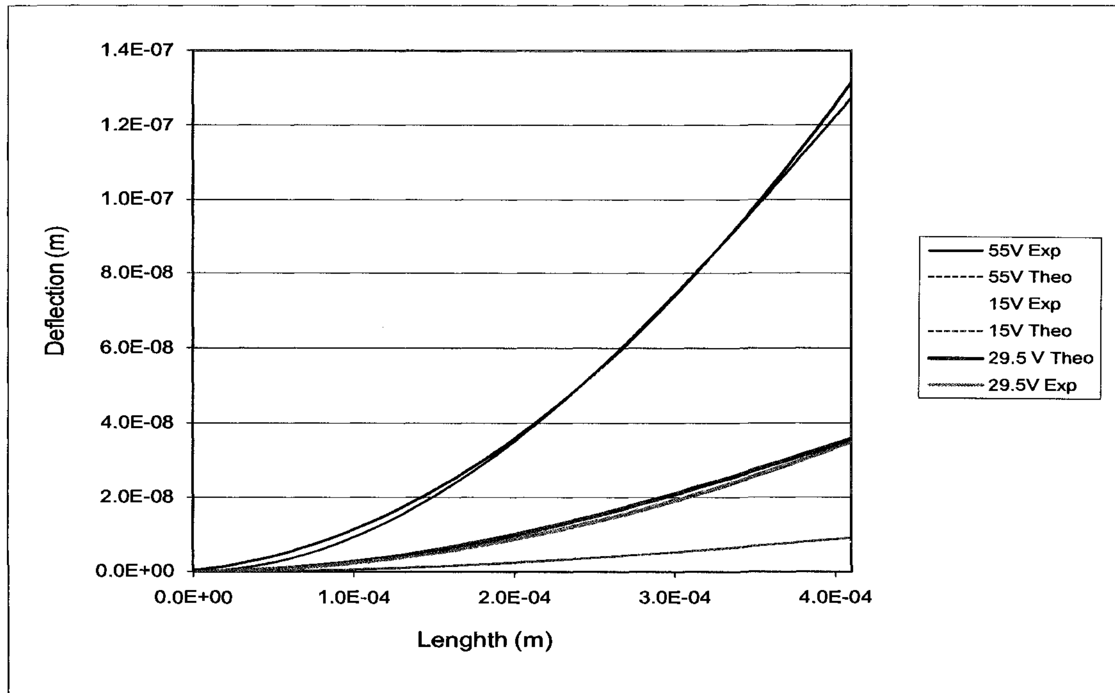

Figure 4.13 Static deflection comparisons

The interferogram obtained depends upon the field of view obtained by the optical system employed. In this regard, the field of view for the AOMSI employed in this work was limited to 410μm. Hence, the results for the static deflections shown in Figure 4.10 are truncated due to this limitation of the optical system. In this regard, a deviation between theoretical and experimental values of ~3% was calculated for the 55V, 29.5V and ~9% for 15V deflection. Below in Table 4.1 are the tabulated results between the experimental and theoretical with its error percentage. The variations between the theory and

experimental results are due, in part, to optical effects related to the surface effects of the reference mirrors. Commercial interferometers employ traceable reference mirrors for higher accuracy. Since in this setup a normal $\lambda/10$ mirror is used as a reference the resolution of the measurement system is ~10nm. The results tabulated below show clearly the reliability of measurement above 10nm. However, the results in themselves demonstrate very good agreement with the analytical model, thereby demonstrating the sensitivity of the detection methodology and also the suitability of employing this approach for microstructure static analysis.

Voltage	**Magnitude of Tip deflection (nm) at 410 μm (Theoretical)**	**Magnitude of Tip deflection (nm) (Experimental)**	**Error**
15V	9.12	8.01	~9%
29.5V	36	34.8	~3%
55V	126	130	~3%

Table 4.1 Tip deflection of the DUT for static characterization

4.6 Summary

Experiments were done for surface profiling on a micro-mirror. 2D and 3D profiles of the micro-mirror and the connecting pads were measured. The out-of-plane curvature profiled was attributed to the internal stress formation on free-standing microstructures. Static characterization methodology and experimental results were presented on micro-cantilever vibrating at 5% of their natural frequency. The results of low frequency static characterization found to be in good agreement with the theoretical predictions.

Chapter 5

Dynamic Characterization

5.1 Introduction

Presented in this chapter are the experimental studies of dynamic behavior on AFM cantilever. The length, width and thickness of the test structure are 350μm, 35μm and 1μm, respectively. The density of the single-crystal-silicon used is 2330kgm^{-3} with an elastic modulus of 169.5 GPa. The methodology and process to conduct dynamic test on AOMSI are detailed out. The mode shapes obtained from the experiments are compared with the simulated mode shapes. The SEM image of the device under test (DUT) is show in Figure 5.1

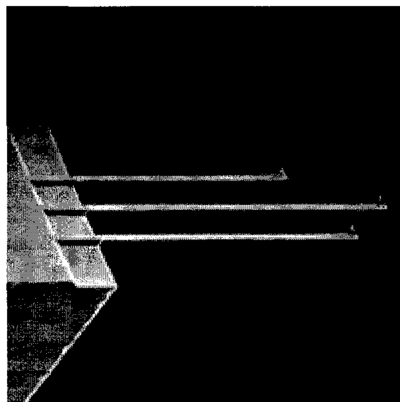

Figure 5.1 SEM image of the AFM Cantilever

5.2 Dynamic Characterization

Dynamic characterization gives the performance evaluation of a device. While performing dynamic characterization on a MEMS device the device performs is investigated in its working state. Due to the extremely small size nature of MEMS device very few tools have been developed (eg: LDV) for understanding the dynamic nature of the MEMS device. AOMSI finds a huge possibility for this type of characterization and has capability to extend it testing capacity to device with higher natural frequency. Compared to other testing method, AOMSI enables high speed visualization of dynamic objects because of its strobing nature. The interferogram of dynamic objects provide higher resolution and higher sensitivity displacement measurements. It can also give details of all the response of the device like various vibration mode shapes.

Figure 5.2 gives details of dynamic characterization on a MEMS device In order to capture the displacement of the device in slow motion there is very small difference δt between the strobing frequency and the driving frequency of the MEMS device. In a periodic motion this difference will help is capturing the motion part by part in a given time frame, so that a standard CCD camera can be used for capturing high-speed motion.

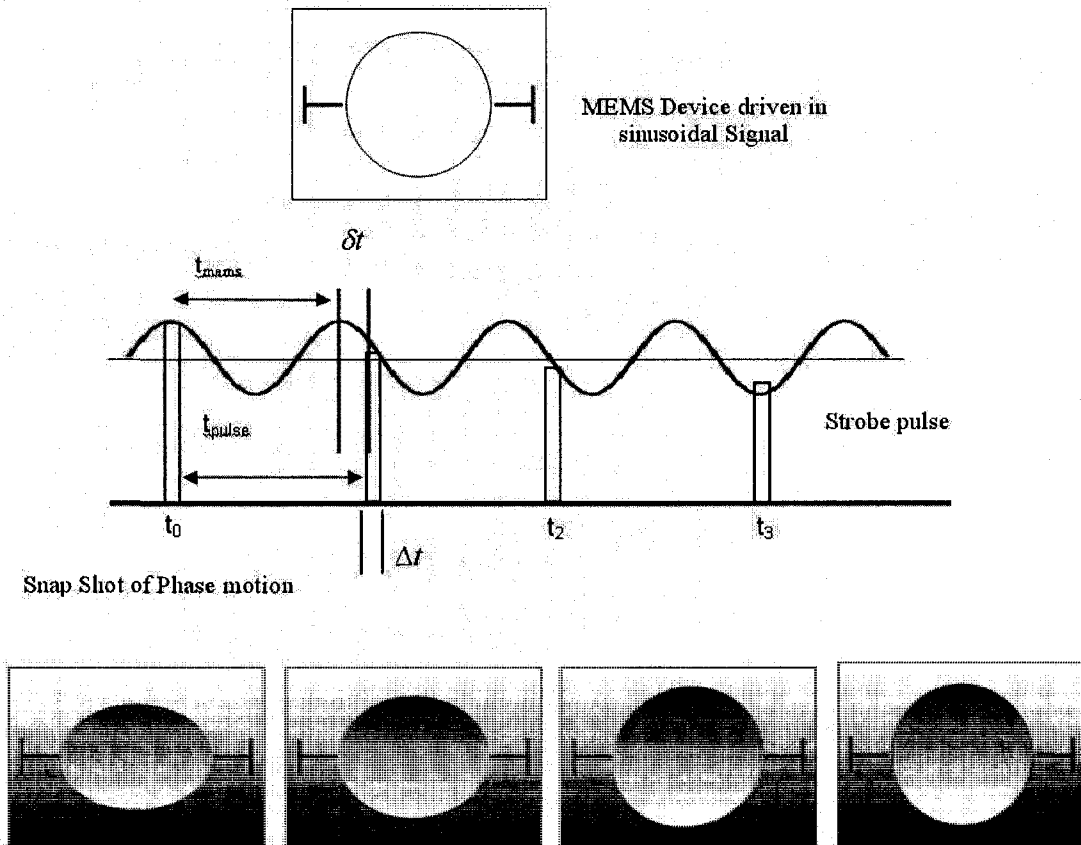

Figure 5.2 Methodology To Conduct Dynamic Characterization

While keeping the same terms as that of static characterization and introducing δt as the difference in the frequency it describe the process in mathematical terms for out-of-plane displacement as follows.

From Equation

$$t_{pulse} - t_{MEMS} = \delta t \tag{5.1}$$

$$t_{pulse} - n2\pi / \omega = \delta t \tag{5.2}$$

$$t_{pulse} = n2\pi / \omega + n\delta t \tag{5.3}$$

For n= 0, 1, 2

$$
\begin{aligned}
t_0 &= \delta t \\
t_2 &= 4\pi / \omega + 2\delta t \\
t_3 &= 6\pi / \omega + 3\delta t
\end{aligned}
\tag{5.4}
$$

From the above equation δt plays a vital role in dynamic characterization. The smaller the δt more the number of frames per cycle. In this work we use frame grabber card so different frames where captured manually. Using a data acquisition card will enable the automation of the image capture to various level of detail. With the developed system dynamic behavior of microdevices actuated by different mechanisms can be studied under various environmental conditions. For example a microcantilever can be actuated either using electro static force or piezo stack to its natural frequency. The system can also be used in vacuum or non-vacuum condition to see the Q-factor of the device.

To prove the concept of dynamic characterization using AOMSI experiments have been conducted on AFM cantilever for detecting its natural frequency and mode shape in its first and second mode of vibrations. The experiments were conducted in non-vacuum conditions. The mode of excitation was using a piezo stage connected to a function generator. The stage was excited using a sinusoidal function.

5.3 Identification of Natural Frequency

The AFM tip is carefully mounted on a piezo stage which is mounted on a six axis stage of the AOMSI. Initially the laser is strobed at higher frequency (1 MHz). The AFM tip is focused with desired number of fringes on it. When the AFM is mounted perfectly the

piezo stage is connected to the function generator for detecting the various natural frequencies of the device. Along with the mode shapes, the 1st and 2nd natural frequencies of the AFM cantilever were also determined. This was achieved, initially, by monitoring the surface motion of the cantilever for a given swept frequency range. The upper bracket of the frequency range was then reduced incrementally in such a manner to obtain a low amplitude surface motion of the device, similarly, the lower frequency bracket was gradually increased to obtain an equal surface displacement as for the upper bracket.

Hence, by using this approach, the shoulders of the resonance frequency response curve were obtained, from which the average of the two values resulted in the center frequency, or resonance frequency of the AFM cantilever. This method was applied for several different lower and upper shoulder values, and an average of the center frequencies obtained was then taken. The experimentally determined 1st and 2nd natural frequencies were 10.7 kHz and 74.6 kHz, respectively. These values are in good agreement with the theoretical values of, 11.2 kHz and 70.4 kHz, for the 1st and 2nd natural frequencies, respectively. The manufacturer supplies a nominal value of 10.0 kHz ± ~3 kHz.

Mode	**Natural Frequency(simulated)**	**Natural frequency (from manufacturer)**	**Natural frequency(Experimental)**
1st	11.2 kHz	10.0 kHz ± ~3 kHz	10.7 kHz
2nd	70.4 kHz	n/a	74.6 kHz

Table 5.1 Comparison of natural frequency

5.4 Characterization of mode shapes

To understand the mode shapes experimentally, the device was excited at 10.7kHz and 74.6kHz, respectively. As described earlier, a 30Hz progressive scan CCD camera with 648 x 492 pixels is used to capture the interferogram. The setup allows one to view the microstructure and to evaluate the behavior in real time. This is made possible by the strobing the laser in tandem with the vibrating frequency. Digital image of the AOMSI while testing the mode shape is shown in Figure 5.3.

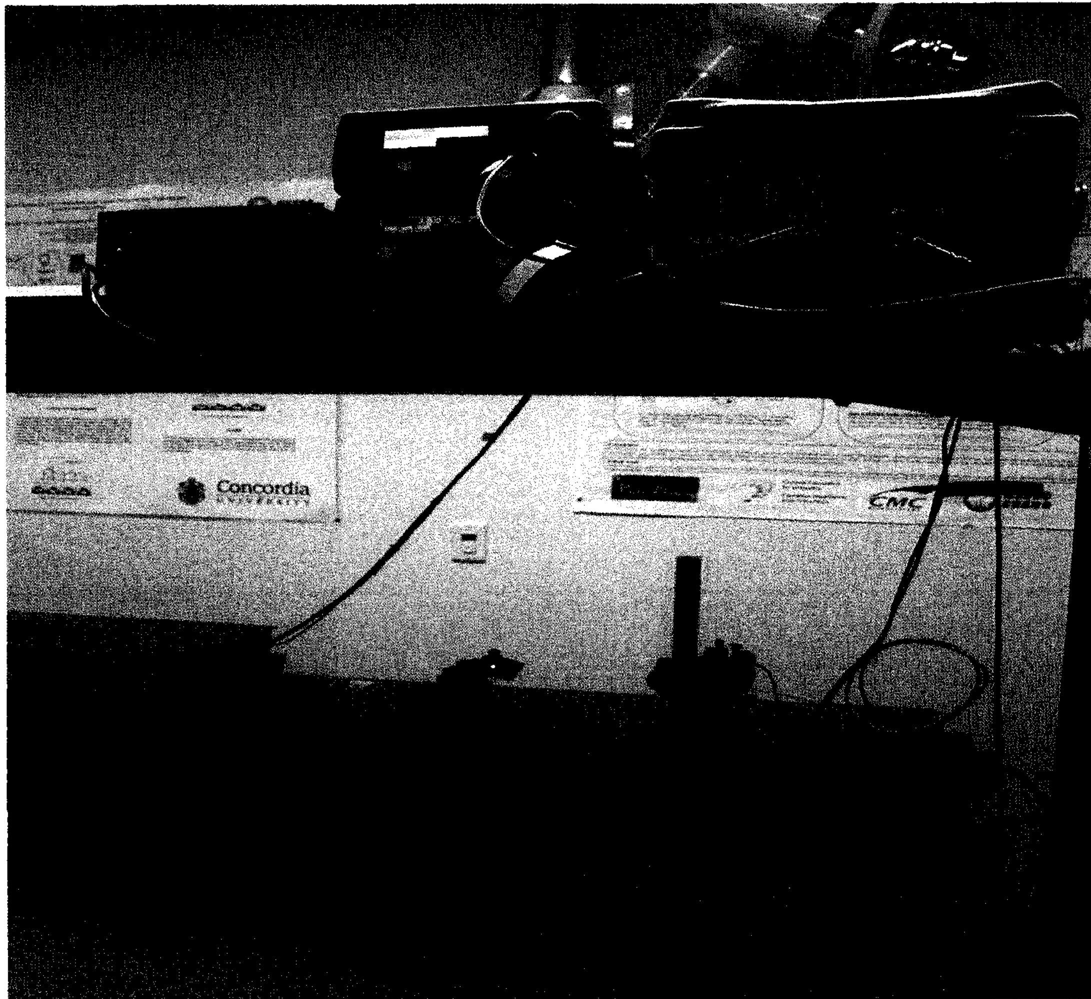

Figure 5.3 Digital image of the interferometer during dynamic characterization

The oscilloscope is used to control the δt to enable manual triggering of the frame grabber card so that the interferograms can be captured at the desired position. Shown in Figure 5.4 are the interference fringes as seen on tipless AFM cantilevers. In this figure, for the middle, and bottom frames the device was driven at the 1st and 2nd resonance frequency, respectively.

For the dynamic flexural mode shapes, the AOMSI method was applied to the AFM cantilever (DUT). In this manner the 1st and 2nd mode shapes were obtained. Higher order modes are also possible; however the limitation of the piezo-excitation source must be considered [2]. Processing the interferogram as described in chapter 4 using Fourier transformation and subsequent filtering, mode shapes of DUT was obtained. Shown in Figure 5.4 is the mode shape of 1st natural frequency at 10.7 KHz obtained experimentally. The three dimensional mode shape obtained experimentally is compared with the mode shape obtained analytically, shown in Figure 5.5 using Raleigh-Ritz approach as discussed in chapter 2. Similarly experiments where done on 2nd natural frequency of 74.6 KHz, for which experimental and analytical mode shapes are shown in Figure 5.6. For the experimental graphics the size of each pixel corresponds to length of 1.1667μm as discussed in chapter 3 so that the 300 pixels seen correspond to 350μm.

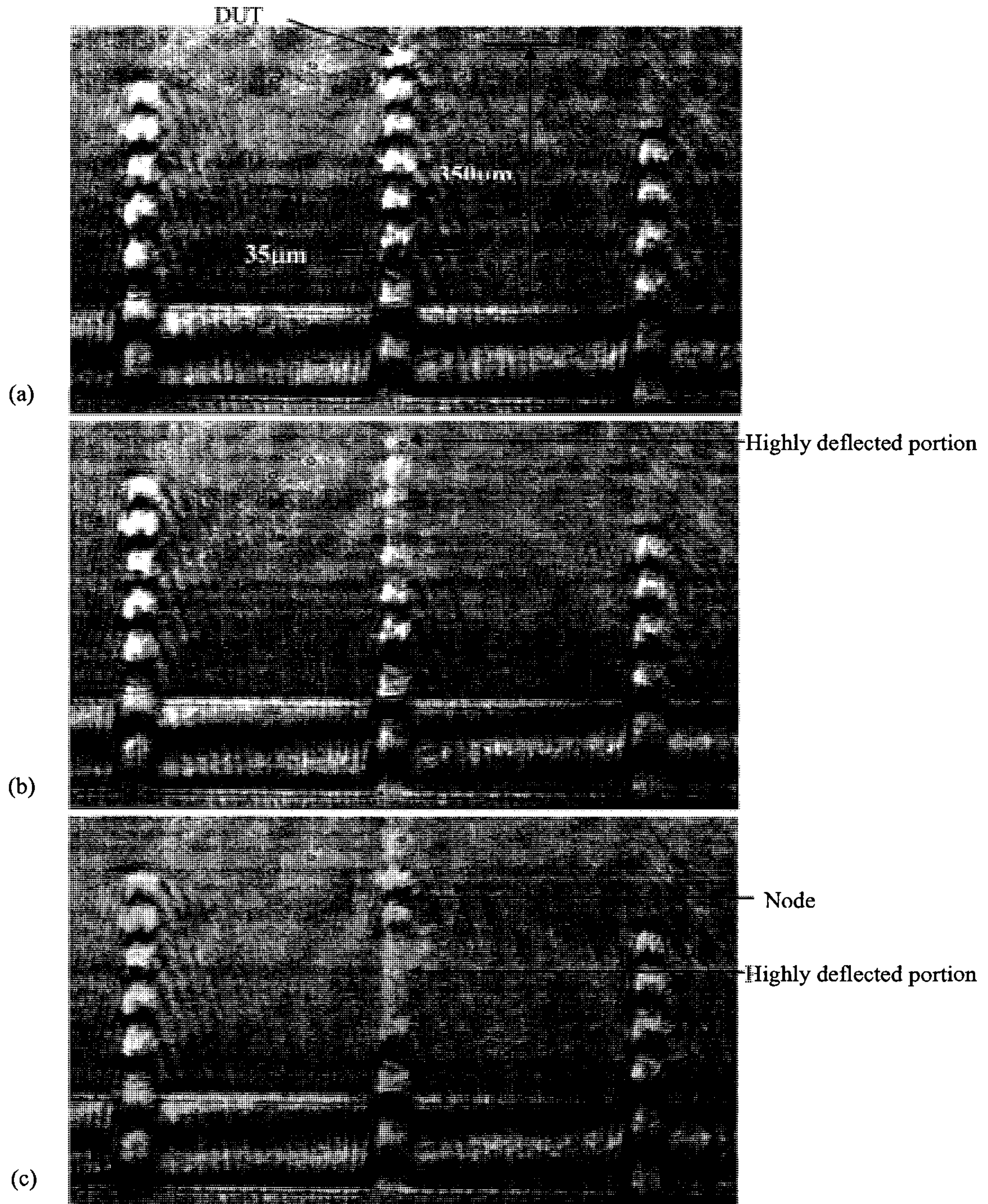

Figure 5.4 The observed fringe pattern obtained seen on AFM cantilevers. a) Device-Under-Test (DUT). b) 1st resonance mode. c) 2nd resonance mode.

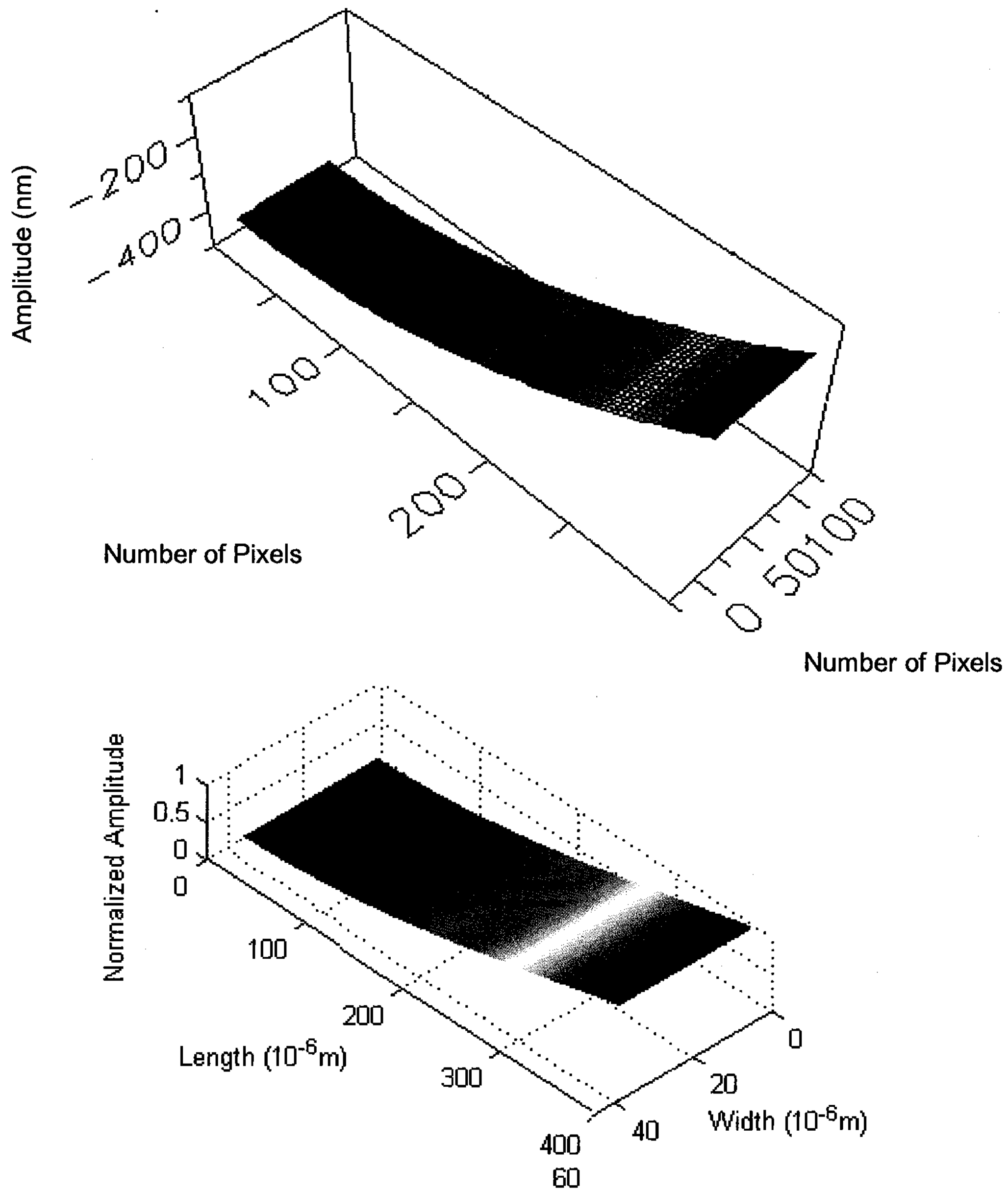

Figure 5.5 Top: AOMSI Surface profile of a resonating AFM cantilever in the 1st mode. Bottom: Analytical representation of the 1st mode shape.

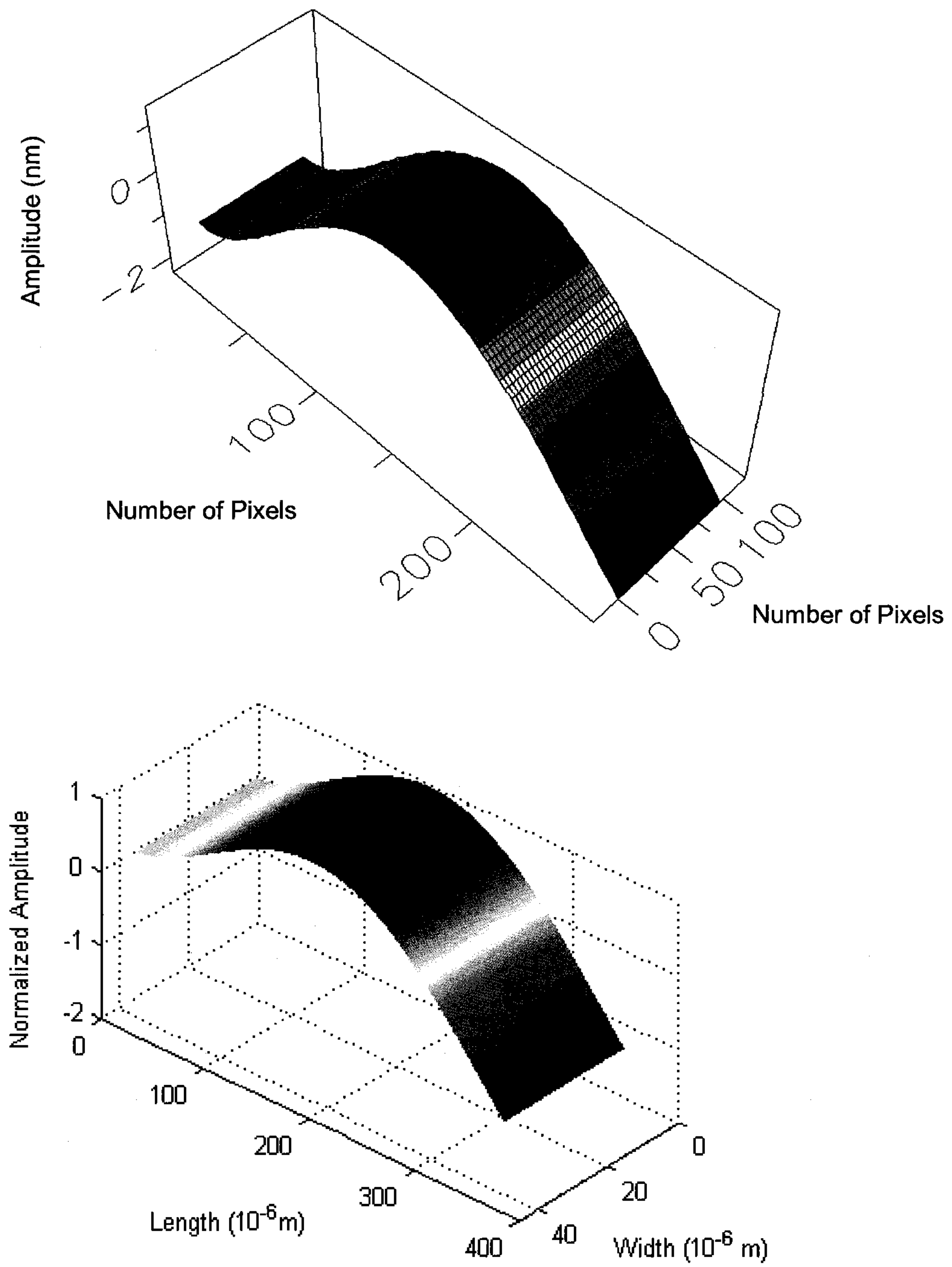

Figure 5.6 Top: AOMSI surface profile of a resonating AFM cantilever in the 2nd mode. Bottom: Analytical representation of the 2nd mode shape.

5.5 Summary

Experiments were done to characterize the dynamic behavior of AFM cantilever. Experimental methodology for identifying the natural frequency was presented. The experimentally determined 1st and 2nd natural frequencies were found to be within the manufacturer's specification and the theoretical predictions. Further experiments were done to profile the 1st and 2nd mode shapes. The normalized mode shapes obtained experimentally were in good agreement with those obtained from the theoretical model.

Chapter 6

Conclusion

6.1 Conclusion

Design and modeling of a simple MEMS device was simulated to understand the mechanical influence on its static and dynamic behavior using Raleigh-Ritz method. A simple yet viable Acousto Optic Modulated Stroboscopic Interferometer (AOMSI) is developed using a frequency stabilized CW laser together with an Acousto Optic Modulator for comprehensive mechanical characterization. The designed interferometer was setup on a vibration isolation table to conduct experiments on microstructures. The real-time vision system was employed on the interferometer to visualize high speed motion and to capture static images of those motions. An optimized methodology for measurement was established and sensitivity analysis was conducted.

Experiments for surface profiling were done on a micro-mirror. The 2D and 3D profile was measured. The out-of-plane curvature found on the micro-mirror was attributed to internal stress formation in the microstructure. Additional surface characterization on MEMS loose die with pads on them was done. The ability of the stroboscopic interferometry to perform measurements accurately on dynamic microstructures was presented in two scenarios, where the microstructures was made to vibrate at 5% of its natural frequency and static deflection to various DC electrostatic voltages were studies in the low frequency static characterization. The results showed good agreement with the theoretical model. The error in comparison between the experimental and theoretical

static influences was ~3% for deflections higher than 10nm. The errors for tip deflections below 10nm were found to be having a higher error percentage which clearly demonstrates the ability of the experimental tool to measure reliably with a resolution of about 10nm.

To further test the ability of dynamic characterization, an AFM cantilever was excited at its natural frequency and the assessment of dynamic behavior was demonstrated. Identifying the natural frequency and modal profile for 1st and 2nd resonance frequencies was carried out. The comparison with the theoretical model showed good agreement and reliability of the AOMSI for investigation of dynamic parameters. The experimental methodology mentioned above explored the feasibility of conducting Fourier transform for fringe processing on a stroboscopic interferometer. The approach is first of its kind developed to investigate the surface, static and dynamic behavior of microstructures using a single tool. Thus the concept of single multi-functional tool to conduct comprehensive mechanical characterization on microstructures was developed.

6.2 Future Work

From the perspective of high precision metrology, objective for improvisation to build and design better characterization tool, opened new approaches on various stands and a few of them are discussed further in recommendation for future work.

Acousto Optic Modulated Stroboscopic Interferometer was built on a vibration isolation table. The setup was developed using open optics with an array of lens and mirrors. The

main constraint was alignment of the optical path through these arrays of optics. It gave us the advantage on various fronts to modify and change the design during the setup. Since the concept is in the stage of maturity, implementation of fiber-optic in AOMSI is a good advancement. It makes its more compact, portable and improves spatial resolution of the tool, in addition to removing noises due to reflections from the various free space optics. To improve the resolution of the AOMSI one of the recommendation is implementation of spatial phase-shifting method. It complicates the experimental setup to a certain extend but can be compromised on for higher out-of-plane resolution to an order of ~ 0.1 to 1 nm. During the post processing of interferogram various image filtering technique were implemented to compensate on the surface profile effect of the reference mirror ($\lambda/10$). A solution to enhance the resolution and also improve the tool would be implementation of a reference mirror that has traceability [106] to National Standards, as is done in commercial interferometers. AOMSI has modulation capability of 4 MHz as designed, but this can be improved up to 85 MHz by implementing a focus system in front of the AOM to reduce the beam diameter of the laser.

References

[1] Rebello, K.J.,(2004), "Applications of MEMS in Surgery" *Proc IEEE,* **92**(1), pp.43-55.

[2] www.piezomechanik.com,(2006), "Piezomechnik technical data sheet"(chk:March2008)

[3] Smith, C.S.,(1954), "Piezoresistance Effect in Germanium and Silicon" *Physical Review,* **94**(1), pp.42-49.

[4] Oliver, W. and Pharr, G.,(1992), "An Improved Technique for Determining Hardness and Elastic Modulus Using Load and Displacement Sensing Indentation Experiments" *J.Mater.Res.,* **7**(6), pp.1564-1583.

[5] Knapp, J.,(1999), "Finite-element modeling of nanoindentation" *J.Appl.Phys.,* **85**(3), pp.1460.

[6] Rinaldi, G., Packirisamy, M. and Stiharu, I.,(2006), "Boundary characterization of microstructures through thermo-mechanical testing" *J Micromech Microengineering,* **16**(3), pp.549-556.

[7] French, P. and Evans, A.,(1985), "Polycrystalline Silicon Strain Sensors" ECS.

[8] Hogarth, C.,(1964), "Semiconductor transducers" *British Journal of Applied Physics,* **15**(2), pp.121-130.

[9] Petersen, K.,(1982), "Silicon as a mechanical material" *Proc IEEE,* **70**(5), pp.420-457.

[10] Hirano, T., Furuhata, T., Gabriel, K. and Fujita, H.,(1992), "Design, fabrication, and operation of submicron gap comb-drivemicroactuators" *Microelectromechanical Systems, Journal of,* **1**(1), pp.52-59.

[11] Yamaguchi, M. And Kawaguchi, S.,(2006), "Study of experimental mechanical stress characterization of MEMS by using of confocal laser scanning microscope with a Raman spectroscopy interface", pp.21-35.

[12] Angell, J., Barth, P. and Terry, S.,(1983), "Silicon micromechanical devices" *Sci.Am.,* **248**pp.44-55.

[13] Lee, J.D., Yoon, J.B., Kim, J.K., Chung, H.J., Lee, C.S., Lee, H.D., Lee, H.J., Kim, C.K. and Han, C.H.,(1999), "A thermal inkjet printhead with a monolithically fabricated nozzleplate and self-aligned ink feed hole" *Microelectromechanical Systems, Journal of,* **8**(3), pp.229-236.

[14] Petersen, K.,(1979), "Fabrication of an integrated, planar silicon ink-jet structure" *Electron Devices, IEEE Transactions on,* **26**(12), pp.1918-1920.

[15] Fan, L.S., Tai, Y.C. and Muller, R.,(1989), "IC-processed electrostatic micromotors." *Sensors Actuators.,* **20**(1), pp.41-47.

[16] Feynman, R.,(2002), "There's Plenty Of Room At The Bottom" *Feynman and Computation: Exploring the Limits of Computers,*

[17] Kim, S., Barbastathis, G. and Tuller, H.,(2004), "MEMS for Optical Functionality" *Journal of Electroceramics,* **12**(1), pp.133-144.

[18] Fujita, H.,(1997), "A decade of MEMS and its future" *Micro Electro Mechanical Systems, 1997.MEMS'97, Proceedings, IEEE., Tenth Annual International Workshop on,* pp.1-7.

[19] Yazdi, N., Salian, A. and Najafi, K.,(1999), "A high sensitivity capacitive microaccelerometer with afolded-electrode structure" *Micro Electro Mechanical Systems, 1999.MEMS'99.Twelfth IEEE International Conference on,* pp.600-605.

[20] Yazdi, N. and Najafi, K.,(2000), "An all-silicon single-wafer micro-g accelerometer with a combined surface and bulk micromachining process" *J Microelectromech Syst,* **9**(4), pp.544-550.

[21] Loh, N., Schmidt, M. and Manalis, S.,(2002), "Sub-10 cm 3 interferometric accelerometer with nano-gresolution" *Microelectromechanical Systems, Journal of,* **11**(3), pp.182-187.

[22] Rinaldi, G., Packirisamy, M. and Stiharu, I.,(2004), "Electrostatic boundary conditioning of MEMS devices" *Proceedings of the 8 thInternational Cairo University MDP, Conference on Current Advances in Mechanical Design and Production VIII,* pp.269-276.

[23] Bosseboeuf, A. and Petitgrand, S.,(2003), "Characterization of the static and dynamic behaviour of M(O)EMS by optical techniques: status and trends" *J.Micromech.Microeng,* **13**(4), pp.s23-s33.

[24] Danilatos, G.,(1988), "Foundations of environmental scanning electron microscopy" *Advances in electronics and electron physics,* **71**pp.109-250.

[25] Gu, M.,(1996), "Principles of Three Dimensional Imaging in Confocal Microscopes" ISBN 9810225504.

[26] Ehrmann, K., Ho, A. and Schindhelm, K.,(1998), "A 3 D optical profilometer using a compact disc reading head" *Measurement Science and Technology,* **9**(8), pp.1259-1265.

[27] Quan, C., Wang, S. and Tay, C.,(2006), "Nanoscale surface deformation inspection using FFT and phase-shifting combined interferometry" *Precis Eng,* **30**(1), pp.23-31.

[28] Krehl, P., Engemann, S., Rembe, C. and Hofer, E.,(1999), "High-speed visualization, a powerful diagnostic tool for microactuators-retrospect and prospect" *Microsystem Technologies,* **5**(3), pp.113-132.

[29] Hart, M., Conant, R., Lau, K. and Muller, R.,(2000), "Stroboscopic interferometer system for dynamic MEMS characterization" *Microelectromechanical Systems, Journal of,* **9**(4), pp.409-418.

[30] Rembe, C., Kant, R. and Muller, R.S.,(2001), "Optical measurement methods to study dynamic behavior in MEMS" *Proc.SPIE,* **4400**pp.127-137.

[31] Rembe, C. and Muller, R.,(2002), "Measurement system for full three-dimensional motion characterization of MEMS" *Microelectromechanical Systems, Journal of,* **11**(5), pp.479-488.

[32] Osten, W. and Ferraro, P.,(2006), "O Digital Holography and Its Application in MEMS/MOEMS Inspection" *Optical Inspection of Microsystems,*

[33] Colomb, T., Marquet, P., Charrière, F., Kühn, J., Jourdain, P., Depeursinge, C., Rappaz, B., Magistretti, P., Prilly, S. and Lausanne, S.,"Electronic Imaging & Signal Processing Enhancing the performance of digital holographic microscopy"

[34] Ngoi, B.K.A., Venkatakrishnan, K. and Tan, B.,(2000), "Laser scanning heterodyne-interferometer for micro-components" *Opt.Commun.,* **173**(1-6), pp.291-301.

[35] Ngoi, B.K.A., Venkatakrishnan, K., Tan, B., Noël, N., Shen, Z. and Chin, C.,(2000), "Two-axis-scanning laser Doppler vibrometer for microstructure" *Opt.Commun.,* **182**(1-3), pp.175-185.

[36] Ono, N., Kitamura, K., Nakajima, K. and Shimanuki, Y.,(2000), "Measurement of Young's Modulus of Silicon Single Crystal at High Temperature and Its Dependency on Boron Concentration Using the Flexural Vibration Method" *Jpn.J.Appl.Phys,* **39**pp.368–371.

[37] Rinaldi, G., Packirisamy, M. and Stiharu, I.,(2007), "Dynamic testing of micromechanical structures under thermo-electro-mechanical influences" *Measurement,* **40**(6), pp.563-574.

[38] Stanbridge, A.B., Martarelli, M. and Ewins, D.J.,(2004), "Measuring area vibration mode shapes with a continuous-scan LDV" *Measurement,* **35**(2), pp.181-189.

[39] Nakadate, S., Saito, H. and Nakajima, T.,(1986), "Vibration Measurement Using Phase-shifting Stroboscopic Holographic Interferometry" *Journal of Modern Optics,* **33**(10), pp.1295-1309.

[40] Rembe, C., Tibken, B. and Hofer, E.,(2001), "Analysis of the dynamics in microactuators using high-speed cinephotomicrography" *Microelectromechanical Systems, Journal of,* **10**(1), pp.137-145.

[41] Yang, L. and Colbourne, P.,(2003), "Digital laser microinterferometer and its applications" *Optical Engineering,* **42**pp.1417.

[42] Kujawinska, M.,"Optical metrology: from micromeasurements to multimedia"

[43] Bracewell, R. and Kahn, P.B.,(1966), "The Fourier Transform and Its Applications" *American Journal of Physics,* **34**pp.712.

[44] Brigham, E.O.,(1988), "The fast Fourier transform and its applications"

[45] Hariharan, P., Oreb, B. and Eiju, T.,(1987), "Digital phase-shifting interferometry: a simple error-compensating phase calculation algorithm" *Appl.Opt.,* **26**(13), pp.2504-2506.

[46] Schmit, J. and Creath, K.,(1995), "Extended averaging technique for derivation of error-compensating algorithms in phase-shifting interferometry" *Appl.Opt.,* **34**(19), pp.3610-3619.

[47] Brophy, C.P.,(1990), "Effect of intensity error correlation on the computed phase of phase-shifting interferometry." *Journal of the Optical Society of America A: Optics and Image Science, and Vision,* **7**(4), pp.537-541.

[48] Takeda, M., Ina, H. and Kobayashi, S.,(1982), "Fourier-transform method of fringe-pattern analysis for computer-based topography and interferometry" *J.Opt.Soc.Am.,* **72**(1), pp.156-160.

[49] Kreis, T.,(1986), "Digital holographic interference-phase measurement using the Fourier- transform method" *Optical Society of America, Journal, A: Optics and Image Science,* **3**pp.847-855.

[50] Bhat, R.,(1985), "Natural frequencies of rectangular plates using characteristic orthogonal polynomials in Rayleigh-Ritz method" *J.Sound Vibrat.,* **102**pp.493-499.

[51] Lam, K., Hung, K. and Chow, S.,(1989), "Vibration analysis of plates with cutouts by the modified Rayleigh-Ritz method" *Appl.Acoust.,* **28**pp.49-60.

[52] Liew, K., Kitipornchai, S., Leung, A. and Lim, C.,(2003), "Analysis of the free vibration of rectangular plates with central cut-outs using the discrete Ritz method" *Int.J.Mech.Sci.,* **45**(5), pp.941-959.

[53] Backus, S., Durfee III, C.G., Murnane, M.M. and Kapteyn, H.C.,(1998), "High power ultrafast lasers" *Rev.Sci.Instrum.,* **69**pp.1207.

[54] Mundkur, G., Bhat, R. and Neriya, S.,(1994), "Vibration Of Plates With Cut-Outs Using Boundary Characteristic Orthogonal Polynomial Functions In The Rayleigh-ritz Method" *J.Sound Vibrat.,* **176**(1), pp.136-144.

[55] Hoffnagle, J.A. and Jefferson, C.M.,(2000), "Design and performance of a refractive optical system that converts a Gaussian to a flattop beam" *Appl.Opt.,* **39**(30), pp.5488–5499.

[56] Hasman, E., Bomzon, Z., Niv, A., Biener, G. and Kleiner, V.,(2002), "Polarization beam-splitters and optical switches based on space-variant computer-generated subwavelength quasi-periodic structures" *Opt.Commun.,* **209**(1-3), pp.45-54.

[57] Gizzi, L.A., Giulietti, D., Giulietti, A., Audebert, P., Bastiani, S., Geindre, J.P. and Mysyrowicz, A.,(1996), "Simultaneous measurements of hard x-rays and second harmonic emission in fs laser-target interactions" *Phys.Rev.Lett.,* **76**(13), pp.2278-2281.

[58] Breton, P.,(1999), "From Microns to Nanometers: Early Landmarks in the science of Scanning Electron Microscope imaging" *Scanning Microsc.,* **13**(1), pp.1-6.

[59] Zhong, W., Overney, G. and Tománek, D.,(1991), "Limits of resolution in atomic force microscopy images of graphite" *Europhys.Lett.,* **15**pp.49.

[60] Binnig, G., Quate, C. and Gerber, C.,(1986), "Atomic Force Microscope" *Phys.Rev.Lett.,* **56**(9), pp.930-933.

[61] Cloud, G.L.,(1995), "Optical Methods of Engineering Analysis" ISBN 0521636426.

[62] Petitgrand, S., Yahiaoui, R., Danaie, K., Bosseboeuf, A. and Gilles, J.,(2001), "3D measurement of micromechanical devices vibration mode shapes with a stroboscopic interferometric microscope" *Optics and Lasers in Engineering,* **36**(2), pp.77-101.

[63] Kwon, O., Shough, D. And Williams, R.,(1987), "Stroboscopic phase-shifting interferometry" *Opt.Lett.,* **12**(11), pp.855-857.

[64] Sreenivasan, M.M.P., Sivakumar, N. and Packirisamy, M.,(2006), "Theoretical modeling of acousto-optic modulated stroboscopic interferometer" *Proceedings of SPIE,* **6343**pp.634322.

[65] Goutzoulis, A.P.,(1994), "Design and Fabrication of Acousto-Optic Devices" ISBN 082478930X.

[66] Kodama, Y., Romagnoli, M. and Wabnitz, S.,(1994), "Stabilisation of optical solitons by an acousto-optic modulator andfilter" *Electron.Lett.,* **30**(3), pp.261-262.

[68] Eldada, L.,(2001), "Advances in telecom and datacom optical components" *Optical Engineering,* **40**pp.1165.

[69] Chang, I.,(1976), "I. Acoustooptic Devices and Applications" *Sonics and Ultrasonics, IEEE Transactions on,* **23**(1), pp.2-21.

[70] Matsumoto, H. and Hirai, A.,(1999), "A white-light interferometer using a lamp source and heterodyne detection with acousto-optic modulators" *Opt.Commun.,* **170**(4-6), pp.217-220.

[71] Lawrence, E.M., Speller, K. and Yu, D.,(2002), "Laser Doppler vibrometry for optical MEMS" *Proceedings of the 5th International Conference on Vibration Measurements by Laser Techniques.Ancona, Italy,* pp.18-21.

[72] Speller, K.E., Goldberg, H., Gannon, J. and Lawrence, E.,"Unique MEMS Characterization Solutions Enabled by Laser Doppler Vibrometer Measurements" *Applied MEMS Inc,* **12200**pp.77477-72409.

[73] Xing, F., Yun-qiang, L. and Xiao-dong, H.,(2004), "Micro laser Doppler vibrometer technology for MEMS dynamic measurement" *Journal of Optoelectronics· Laser,* **15**(11), pp.1357-1360.

[74] Pister, K.S.J.,"Introduction to MEMS Design and Fabrication" *EECS,* **245**pp.9-45.

[75] Judy, J.W.,(2001), "Microelectromechanical systems(MEMS)- Fabrication, design and applications" *Smart Mater Struct,* **10**(6), pp.1115-1134.

[76] Bao, M. and Wang, W.,(1996), "Future of microelectromechanical systems (MEMS)" *Sensors & Actuators: A.Physical,* **56**(1-2), pp.135-141.

[77] Madou, M.J.,(1997), "Fundamentals of microfabrication" ISBN 0849394511

[78] Madou, M.J.,(2002), "Fundamentals of Microfabrication: The Science of Miniaturization" ISBN 0849308267

[79] Noell, W., Clerc, P.A., Dellmann, L., Guldimann, B., Herzig, H.P., Manzardo, O., Marxer, C., Weible, K., Dandliker, R. and de Rooij, N.,(2002), "Applications of SOI-based optical MEMS" *Selected Topics in Quantum Electronics, IEEE Journal of,* **8**(1), pp.148-154.

[80] Kovacs, G.T.A., Maluf, N.I. and Petersen, K.E.,(1998), "Bulk micromaching of silicon" *Proc IEEE,* **86**(8), pp.1536–1551.

[81] Howe, R.T.,(1988), "Surface micromachining for microsensors and microactuators" *Journal of Vacuum Science & Technology B: Microelectronics and Nanometer Structures,* **6**pp.1809.

[82] Bustillo, J., Howe, R. and Muller, R.,(1998), "Surface micromachining for microelectromechanical systems" *Proc IEEE,* **86**(8), pp.1552-1574.

[83] Rinaldi, G., Packirisamy, M. and Stiharu, I.,(2007), "Quantitative Boundary Support Characterization for Cantilever MEMS" *Sensors,* **7**pp.2062-2079.

[84] Brown, G.C. and Pryputniewicz, R.J.,(2000), "New test methodology for static and dynamic shape measurements of microelectromechanical systems" *Optical Engineering,* **39**pp.127.

[85] Grigg, D., Felkel, E., Roth, J., de Lega, X.C., Deck, L. and de Groot, P.J.,(2004), "Static and dynamic characterization of MEMS and MOEMS devices using optical interference microscopy" *Proceedings of SPIE,* **5455**pp.429-435.

[86] Arney, S.,(2001), "Designing for MEMS reliability" *MRS Bull,* **26**(4), pp.296-299.

[87] Espinosa, H., Prorok, B. and Fischer, M.,(2003), "A methodology for determining mechanical properties of freestanding thin films and MEMS materials" *J.Mech.Phys.Solids,* **51**(1), pp.47-67.

[88] Chiao, M. and Lin, L.,(2000), "Self-buckling of micromachined beams under resistive heating" *Microelectromechanical Systems, Journal of,* **9**(1), pp.146-151.

[89] Pelesko, J.A. and Bernstein, D.H.,(2003), "Modeling MEMS and NEMS" ISBN 1584883065

[90] Matey, J.R.,(1984), *Scanning capacitance microscope,* Patent number: 4481616

[91] Binnig, G. and Rohrer, H.,(1986), "Scanning tunneling microscopy" *IBM Journal of Research and Development,* **30**(4), pp.355-369.

[92] Schroder, D.K.,(1990), "Semiconductor material and device characterization"

[93] Shrewsbury, P., Muller, S. and Liepmann, D.,(1999), "Characterization of DNA Flow through Microchannels" *Technical Proceedings of the 1999 International Conference on Modeling and Simulation of Microsystems,* pp.578–580.

[94] Wyant, J.,(1982), "Interferometric Optical Metrology: Basic Principles and New Systems." *Laser Focus(Includes Electro-Optics),* **18**(5), pp.65-71.

[95] Born, M. and Wolf, E.,(2000), "Principles of Optics: Electromagnetic Theory of Propagation, Interference and Diffraction of Light"

[97] In, L.,"Interferometry: Technology and Applications" Veeco Inc.

[98] Hiller, W., Lent, H.M., Meier, G. and Stasicki, B.,(1987), "A pulsed light generator for high speed photography" *Exp.Fluids,* **5**(2), pp.141-144.

[99] Hansen, H., Carneiro, K., Haitjema, H. and De Chiffre, L.,(2006), "Dimensional Micro and Nano Metrology" *CIRP Annals-Manufacturing Technology,* **55**(2), pp.721-743.

[100] VanderLugt, A.,(1982), "Bragg cell diffraction patterns" *Appl.Opt.,* **21**pp.1092-1100.

[101] Aswendt, P., Schmidt, C.D., Zielke, D. and Schubert, S.,(2003), "ESPI solution for non-contacting MEMS-on-wafer testing" *Optics and Lasers in Engineering,* **40**(5-6), pp.501-515.

[102] Malacara, D.,(1978), "Twyman-Green Interferometer" *Optical Shop Testing.Edited by Daniel Malacara.Published by John Wiley & Sons, Wiley Series in Pure and Applied Optics, New York, 1978., p.47,*

[103] Yamaguchi, I., Ohta, S. and Kato, J.,(2001), "Surface contouring by phase-shifting digital holography" *Optics and Lasers in Engineering,* **36**(5), pp.417-428.

[104] Osten, W., Elandaloussi, F. and Mieth, U.,(1998), "The bias fringe processor—a useful tool for the automatic processing of fringe patterns in optical metrology" *3rd International Workshop in Optical Metrology-Series in Optical Metrology, Akademie Verlag,* pp.98–107.

[105] Inc, M.,(2004), "Introduction to MicraGeM: A Silicon-on-Insulator Based Micromachining Process"

[106] Leach, R., Haycocks, J., Jackson, K., Lewis, A., Oldfield, S. and Yacoot, A.,(2001), "Advances in traceable nanometrology at the National Physical Laboratory" *Nanotechnology,* **12**(1), pp.R1-R6.

[107] Pawley, J.B.,(1995), "Handbook of Biological Confocal Microscopy"

[108] Mau, A.E. and Young, W.A.,(2003), "Letters to the Editor" *Pain,* **104**pp.426.

Appendix

List of Journal and Conference

I. Murali Pai, Gino Rinaldi, Muthukumaran Packrisamy, N.Sivakumar "**Low Frequency static characterization of microstructure using Acousto-optic modulated stroboscopic inteferometer**" Journal of Optics and Lasers Engineering (Accepted In Print)

II. Murali Pai, Gino Rinaldi, Muthukumaran Packrisamy, N.Sivakumar "**Metrology,Static and Dynamic Charactrization using Acousto-optic modulated stroboscopic inteferometer**" Measurement(2007)(under review)

III. Murali Pai, N.Sivakumar, Muthukumaran Packrisamy, **"Theoretical Modeling of Acousto-Optic Modulated Stroboscopic Interferometer"** Proc. SPIE Vol. 6343.

IV. Murali Pai, N.Sivakumar, Muthukumaran Packrisamy, **"Testing of Static Behavior on Microstructures By Acousto-Optic Modulated Stroboscopic Interferometeric Technique"** Photonic North 2007, Ottawa.(SPIE proceeding In print)

V. Murali Pai, N.Sivakumar, Muthukumaran Packrisamy, **"Acousto-Optic Modulated Stroboscopic Interferometer: Innovative Nano Metrological Tool For Nano And Micro Structures"** NANO 2007, Montreal. Conference held by NanoQuebec.

VI. Murali Pai, N.Sivakumar, Muthukumaran Packrisamy, "**Acousto – Optic Modulated Stroboscopic interferometer for MEMS characterization"** CMC Microsystem 2006 Annual Symposium, Ottawa, 2006.

VII. Murali Pai, N.Sivakumar, Muthukumaran Packrisamy, "**Device Characterization of Dynamic and Static behavior of Microstructure using Acousto Optic Modulated Stroboscopic Interferometer"** CMC Microsystem 2007 MEMS workshop, Montreal.